Monazite-group minerals and xenotime-(Y) in A-type granitic rocks: chemical composition and in-situ Th–U–total Pb EPMA dating (Velence Hills, Hungary)

Tomáš Sobocký[1], Martin Ondrejka[1], Pavel Uher[1], Tomáš Mikuš[2] & Patrik Konečný[3]

[1] Department of Mineralogy and Petrology, Faculty of Natural Sciences, Comenius University in Bratislava, Mlynská dolina, Ilkovičova 6, 842 15, Bratislava, Slovakia; sobocky1@uniba.sk; martin.ondrejka@uniba.sk; pavel.uher@uniba.sk
[2] Earth Science Institute, Slovak Academy of Sciences, Ďumbierska 1, 974 11, Banská Bystrica, Slovakia; mikus@savbb.sk
[3] State Geological Institute of Dionýz Štúr, Mlynská dolina 1, 817 04 Bratislava, Slovakia; patrik.konecny@geology.sk

AGEOS

Abstract: Accessory monazite-(Ce), -(La), -(Nd), cheralite (monazite-group minerals, MGM) and xenotime-(Y) are rare magmatic accessory minerals in subsolvus A-type granites and related aplite and pegmatite dykes in the Velence Hills, Transdanubian Unit, Hungary. The MGM and xenotime-(Y) form ≤ 200 μm euhedral to subhedral crystals in association with allanite-(Ce), zircon, fluorapatite, and ilmenite. Investigated MGM shows dominant cheralite ($Ca^{2+} + Th^{4+} \leftrightarrow 2REE^{3+}$) and subordinate huttonite ($REE^{3+} + P^{5+} \leftrightarrow Th^{4+} + Si^{4+}$) substitution with greater extent in pegmatite and aplite than in the host granite. Monazite in-situ Th–U–total Pb electron-microprobe dating of the Velence granite determined 289 ± 3 Ma age (MSWD = 3.22, n = 62) and this confirmed post-Variscan, Permian, (Cisuralian) magmatic crystallization. In addition, xenotime-(Y) from the same rock samples gave 266 ± 5.2 Ma age (MSWD = 1.4, n = 44), and this corresponds to Permian (Guadalupian) post-magmatic (subsolidus) recrystallization of xenotime-(Y) during a younger event and subsequent overprint of the parental granitic rocks. Although monazite-(Ce) remains relatively unaffected, fluid-induced breakdown of xenotime-(Y) produced numerous tiny thorite and cheralite inclusions in the altered xenotime-(Y) domains which can be formed by coupled dissolution-reprecipitation reactions between orthomagmatic xenotime-(Y) and younger late to post-magmatic granitic fluids.

Key words: monazite, xenotime, EPMA dating, A-type granite, Velence, Hungary

1. INTRODUCTION

Monazite-(Ce) and xenotime-(Y) are accessory phosphate minerals and principal carriers of REE and Y in common magmatic and metamorphic rocks, together with allanite-(Ce), zircon, titanite and fluorapatite. Detailed study of their chemical composition and breakdown processes enables understanding of the processes occurring during petrogenesis and evolution of the parental rock (e.g., Montel, 1993; Uher & Broska, 1995; Bea, 1996; Bingen et al., 1996; Montel et al., 1996; Finger et al., 1998; Broska & Siman, 1998; Förster, 1998; Zhu & O`Nions, 1999; Spear & Pyle, 2002; Johan & Johan, 2005; Finger & Krenn, 2007; Krenn & Finger, 2007; Petrík & Konečný, 2009; Ondrejka et al., 2007, 2012; Uher et al., 2015 and many others).

In addition, REE phosphates (monazite and xenotime) are popular targets for petrochronology (Engi, 2017). The commonly high concentrations of Th and U, low initial Pb (Parrish, 1990), low cation diffusion rates (e.g., Cherniak et al., 2004; Cherniak, 2006) allow chemical U–Th–Pb dating by EPMA (e.g., Suzuki & Adachi, 1991; Suzuki et al., 1991; Montel et al., 1996; Scherrer et al., 2000; Cocherie & Albarede, 2001; Williams et al., 2006; Hetherington et al., 2008; Spear et al., 2009). Similarly, in-situ isotopic dating by LA-ICP-MS and SIMS are suited to link ages with their geochemical and textural content (e.g., Kylander-Clark, 2017; Schmitt & Vazquez, 2017).

Monazite-(Ce) and xenotime-(Y) can also be unstable during post-magmatic and metamorphic fluid-activated overprinting (Budzyń et al., 2010, 2011, 2017, 2018, Budzyń & Sláma, 2019) and both can form subsolidus retrograde allanite-apatite coronas during pervasive fluid-influx (e.g., Broska & Siman, 1998; Finger et al., 1998; Broska et al., 2005; Krenn et al., 2012; Ondrejka et al., 2012, 2016; Upadhyay & Pruseth, 2012; Lo Pò et al., 2016). The redundant amount of Th in monazites in fluid-rock contact can be released and precipitate a further phase (huttonite/thorite, thorianite or cheralite) near the monazite (Harlov et al., 2007; Petrík & Konečný, 2009; Budzyń et al., 2011, 2017; Harlov, 2011; Ondrejka et al., 2012).

However, our knowledge of primary monazite-(Ce) and xenotime-(Y) distribution, their textural and paragenetic relationships and compositional variations is mainly based on the study of these accessory minerals in orogen-related, calc-alkaline S- and I-type granitic suites as well as in orthogneisses and metapelitic to metapsammitic rocks. This also applies to their use as a petrochronological tool for reconstructing their processes and age constraints (e.g., Bea, 1996; Broska et al., 2005, 2012[a], 2012[b]).

Primary magmatic monazite-(Ce) is a characteristic accessory mineral, especially for peraluminous S-type granites, and it is relatively scarce in subaluminous A- and I-type granitic suites where allanite-(Ce) is a dominant REE phase (Bea, 1996; Broska et al., 2012[a]). In contrast, xenotime-(Y) dominantly occurs in peraluminous leucogranites and granitic pegmatites with S- and A-type affinity and more rarely in I-type granites (Demartin et al., 1991[a]; Buck et al., 1999; Broska et al., 2005;

Manuscript received 2019-04-29
Revised version accepted 2020-10-19

Hetherington & Harlov, 2008). This is most likely due to the relatively low LREE/(Y + HREE) ratio or Y + HREE enrichment in those suites. Secondary post-magmatic xenotime-(Y) can form during the late-stage activity of hydrothermal fluids in granites or pegmatites during cooling of the host rock (Åmli, 1975; Hetherington & Harlov, 2008; Harlov, 2011).

This paper documents the magmatic and post-magmatic evolution of monazite-group minerals (MGM) and xenotime-(Y) in A-type granites and their aplite and pegmatite derivatives in the Velence granite massif (Hungary). We identify their textural and paragenetic relationships, the variations in chemical compositions and chemical in-situ Th–U–total Pb dating of both minerals. This provides key information on magma crystallization and post-magmatic processes, including rock-fluid interaction and dating of these geological processes, and it enables better understanding of A-type granite evolution.

2. GEOLOGICAL SETTING

The Velence granite massif (VGM) is located in the Velence Hills, a small and low mountain in the NW part of Hungary, N of Velence Lake and approximately 70 km SW from Budapest. The Velence Hills rocks belong to the Transdanubian Unit, Inner Western Carpathians (*sensu* Plašienka et al., 1997) where the Balaton Lineament forms the southern tectonic border of the hills. Outcrops of the VGM have eastern and western main areas (Fig. 1).

The VGM intruded into Palaeozoic (Ordovician to Devonian) metamorphic rocks (metasediments) of the Lovas Slate Formation. The granitoid rocks are divided into two petrographic suites: coarse-grained porphyric monzogranite and fine-grained biotite-bearing monzogranite. The modal composition of both suites is approximately 32 % quartz, 31% perthitic orthoclase, 32 % plagioclase and 5 % biotite. However, biotite is absent in leucocratic types and the rock colour is light to medium grey (Horváth et al., 2004). The common accessory minerals are fluorapatite, zircon, magnetite, epidote, fluorite, titanite, pyrite and molybdenite (Jantsky, 1957; Buda, 1969, 1985; Buda & Nagy, 1995). The mainly biotite granitic rocks, which commonly have porphyric K-feldspar phenocrysts, are cut by dykes of granite porphyries, aplites and pegmatites (Buda, 1993; Uher & Broska, 1995) and also alkali-ultramafic intrusive bodies including carbonatites and lamprophyres (Horváth et al., 1983). In addition, the VGM in the W and NE part of the Velence Hills is also cut by Eocene volcanites of the Nadap Andesite Formation. The Velence granites have geochemical and tectonic affinity to a post-orogenic or anorogenic A-type granite suite (Uher & Broska, 1996; Broska & Uher, 2001; Uher et al., 2002), and U–Pb zircon dating constrained their Permian age to ≈ 280 Ma (Uher et al., 2009). Various Permian magmatic intrusions occurred in the Inner Western Carpathians: intermediate and basic volcanism (Vozárová et al., 2018), lamprophyre (Spišiak et al., 2018) and granite (Broska & Kubiš, 2018).

3. ANALYTICAL METHODS AND SAMPLE LOCATIONS

The MGM and xenotime-(Y) were analysed by CAMECA SX-100 microprobe at the Department of Electron Microanalysis

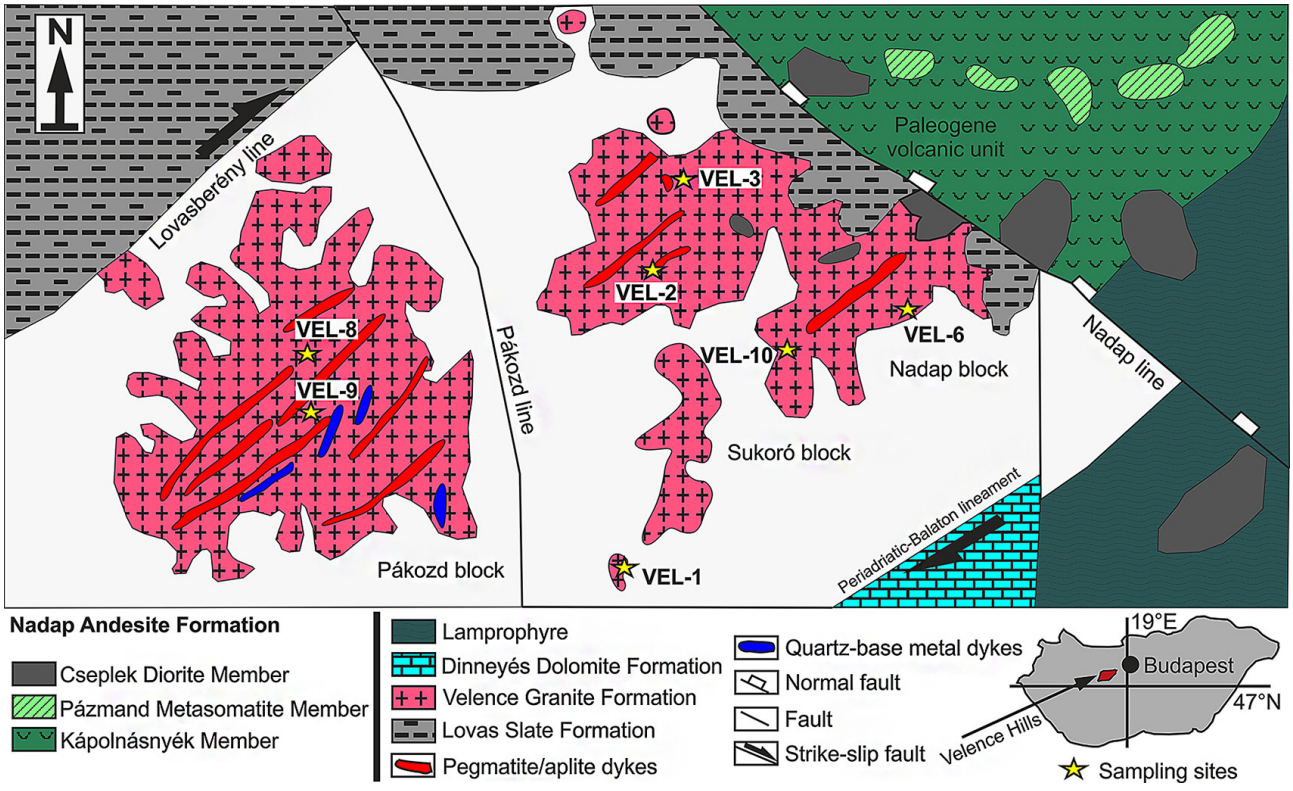

Fig. 1: Geological map of the Velence Hills area with sample locations (modified after Horváth et al., 2004 and Benkó et al., 2010, 2014[a], 2014[b]).

Table 1: Localisation of samples and GPS coordinates.

Sample	Localisation and description of area	Rock type	GPS coordinates
VEL-1	Natural outcrop southwest from Sukoró village	porphyric granite	N: 47°12.636´ E: 18°34.582´
VEL-2F	Outcrop next to military monument near Sukoró village	porphyric granite	N: 47°13.068´ E: 18°34.851´
VEL-2G	Outcrop next to military monument near Sukoró village	banded aplite	N: 47°12.636´ E: 18°34.851´
VEL-3B	Road outcrop next to Sukoró village	aplite	N: 47°13.216´ E: 18°34.790´
VEL-6C	Outcrop behind the transmitter near the road on the E slope of Bence Hill near Nadap village	microgranite	N: 47°19.942´ E: 18°37.615´
VEL-8A	Béllá valley near Pákozd village	aplite	N: 47°12.636´ E: 18°31.38´
VEL-8B	Béllá valley near Pákozd village	aplite	N: 47°12.636´ E: 18°31.38´
VEL-8C	Béllá valley near Pákozd village	aplite	N: 47°12.636´ E: 18°31.38´
VEL-9	Abandoned fluorite quarry near Pákozd village	pegmatite	N: 47°13.721´ E: 18°31.425´
VEL-9A	Abandoned fluorite quarry near Pákozd village	pegmatite	N: 47°13.721´ E: 18°31.425´
VEL-10	Abandoned Rigohégy quarry near Sukoró village	biotite granite	N: 47°14.451´ E: 18°34.926´

at the State Geological Institute of Dionýz Štúr in Bratislava. The analytical conditions used for non-dated mineral phases included 15 kV accelerating voltage, 35–40 nA probe current, 3–10 μm beam diameter and dependent on mineral sensitivity to induced beam damage.

Monazite and xenotime Th–U–total Pb dating conditions comprised 15 kV accelerating voltage, 180 nA probe current and 3 μm beam diameter. Finally, the PAP matrix correction factors were used, and the following conditions are specified in (Tab. 2.) Analytical lines free of overlap were preferentially selected. Mutual interferences among REE were corrected by empirical correction factors. The Pb$M\alpha$ line is overlapped by La$L\alpha$, Th$M\zeta$1, Th$M\zeta$2, and Y$L\gamma$2,3. The weak interference with La$L\alpha$ was neglected. The U$M\beta$ line is overlapped by Th$M\zeta$, ThM3-N4 and ThM5-P3. The Pb$M\alpha$ line overlaps were resolved with consideration of curved exponential background. Monazite dating includes measurement of 7 – 9 age monazite standards and applying of correction dependencies derived from measured compositions. Further details and description of dating procedure named MARC can be found in Konečný et al. (2018). Procedure of xenotime-(Y) dating was slightly modified because of using the Pb$M\beta$. Back-scattered-electron imaging (BSE) was performed by CAMECA SX-100 microprobe at the State Geological Institute of Dionýz Štúr in Bratislava and the JEOL JXA-8530F microprobe at the Earth Science Institute of the Slovak Academy of Sciences in Banská Bystrica. The formula element contents are expressed in atoms per formula unit (apfu), and the MGM and xenotime-(Y) formulae were normalised on 4 oxygen anions.

The investigated samples were collected from 7 different localities. The VEL-1, 2, 3, 6, and 10 samples came from the eastern granite body in the Sukoró area and the VEL-8 and 9 samples from the western granite body in the Pákozd area. Granite samples include leucocratic coarse-grained porphyritic granite with K-feldspar, albite, quartz, and/or biotite. The aplite samples comprise fine-grained quartz, feldspar, and/or biotite, and only one sample contains granitic pegmatite with unequigranular texture and K-feldspar porphyritic phenocrysts. The location of sampling sites with GPS coordinates is presented in Tab. 1.

Table 2: EPMA conditions used for each element.

				Detection limit (3σ) in ppm
Element	**Line**	**Crystal**	**Calibrant**	**MGM and xenotime-(Y)**
S	*Kα*	LPET	baryte	81-262
P	*Kα*	LPET	apatite	105-322
As	*Lα*	TAP	GaAs	485-677
Si	*Kα*	TAP	wollastonite	127-363
Th	*Mα*	LPET	ThO_2	218-569
U	*Mβ*	LPET	UO_2	195-835
Al	*Kα*	TAP	Al_2O_3	127-379
Y	*Lα*	LPET	YPO_4	161-543
La	*Lα*	LLIF	$LaPO_4$	644-1295
Ce	*Lα*	LLIF	$CePO_4$	572-1147
Pr	*Lβ*	LLIF	$PrPO_4$	977-1178
Nd	*Lα*	LLIF	$NdPO_4$	615-1003
Sm	*Lα*	LLIF	$SmPO_4$	722-1247
Eu	*Lβ*	LLIF	$EuPO_4$	1162-1410
Gd	*Lα*	LLIF	$GdPO_4$	759-1155
Tb	*Lα*	LLIF	$TbPO_4$	687-1235
Dy	*Lβ*	LLIF	$DyPO_4$	1417-1741
Ho	*Lβ*	LLIF	$HoPO_4$	1537-1850
Er	*Lβ*	LLIF	$ErPO_4$	1629-1978
Tm	*Lα*	LLIF	$TmPO_4$	788-1393
Yb	*Lα*	LLIF	$YbPO_4$	851-1387
Lu	*Lβ*	LLIF	$LuPO_4$	1541-3066
Ca	*Kα*	LPET	wollastonite	79-263
Sr	*Lα*	LPET	$SrTiO_3$	272-490
Ba	*Lα*	LPET	baryte	417-480
Fe	*Kα*	LIF	fayalite	402-1159
Mn	*Kα*	LLIF	rhodonite	902-1086
Pb	*Mα, β*	LPET	$PbCO_3$	92-677
Na	*Kα*	TAP	albite	410-683
K	*Kα*	LPET	orthoclase	85-251
F	*Kα*	LPC0	CaF_2	584-754
Cl	*Kα*	LPET	NaCl	232-271

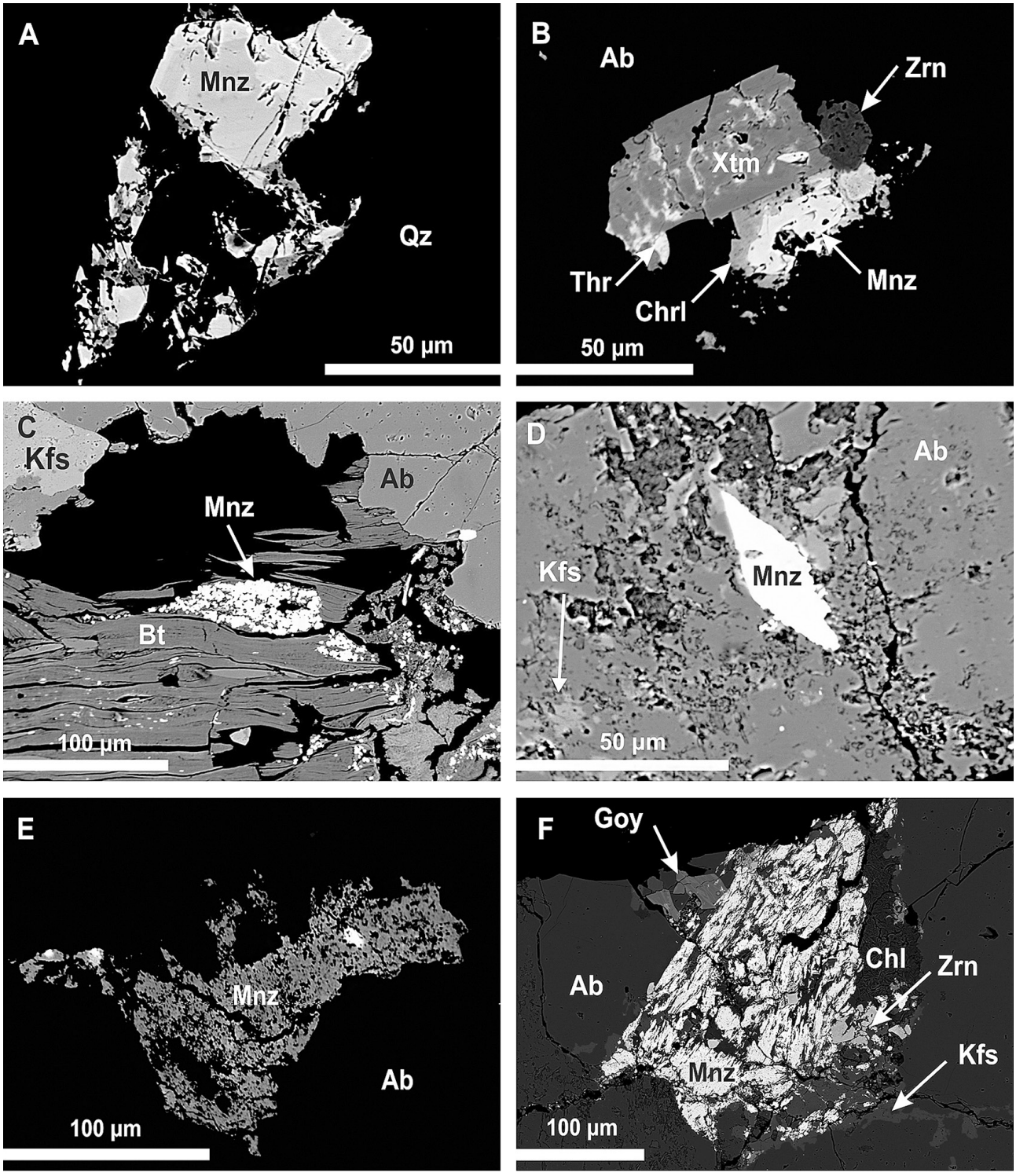

Fig. 2: Back-scattered electron (BSE) images of MGM and associated minerals. A – Anhedral aggregate of monazite-(Ce) – (Mnz) in quartz (Qz), where brighter domains are Th-rich. Sample VEL-2F (granite). B – Accessory mineral assemblage of monazite-(Ce) – (Mnz), xenotime-(Y) – (Xtm) with cheralite (Chrl) and thorite (Thr) inclusions and zircon (Zrn) in albite (Ab). Sample VEL-2F (granite). C – Rare glomeroporphyric aggregate (synneusis) of monazite-(Ce) – (Mnz) in biotite (Bt). Sample VEL-2F (granite). D – Solitary euhedral crystal of monazite-(Ce) – (Mnz) in albite (Ab). Sample VEL-2F (granite). E – Anhedral aggregate of MGM (Mnz) in albite (Ab). Sample VEL-9 (pegmatite). F – Large aggregate of hydrated(?) MGM (Mnz) or possible rhabdophane in association with zircon (Zrn), albite (Ab) and K-feldspar (Kfs). Secondary minerals are represented by chlorite (Chl) and rare secondary goyazite (Goy). Sample VEL-9 (pegmatite). Mineral abbreviations are after Whitney & Evans (2010).

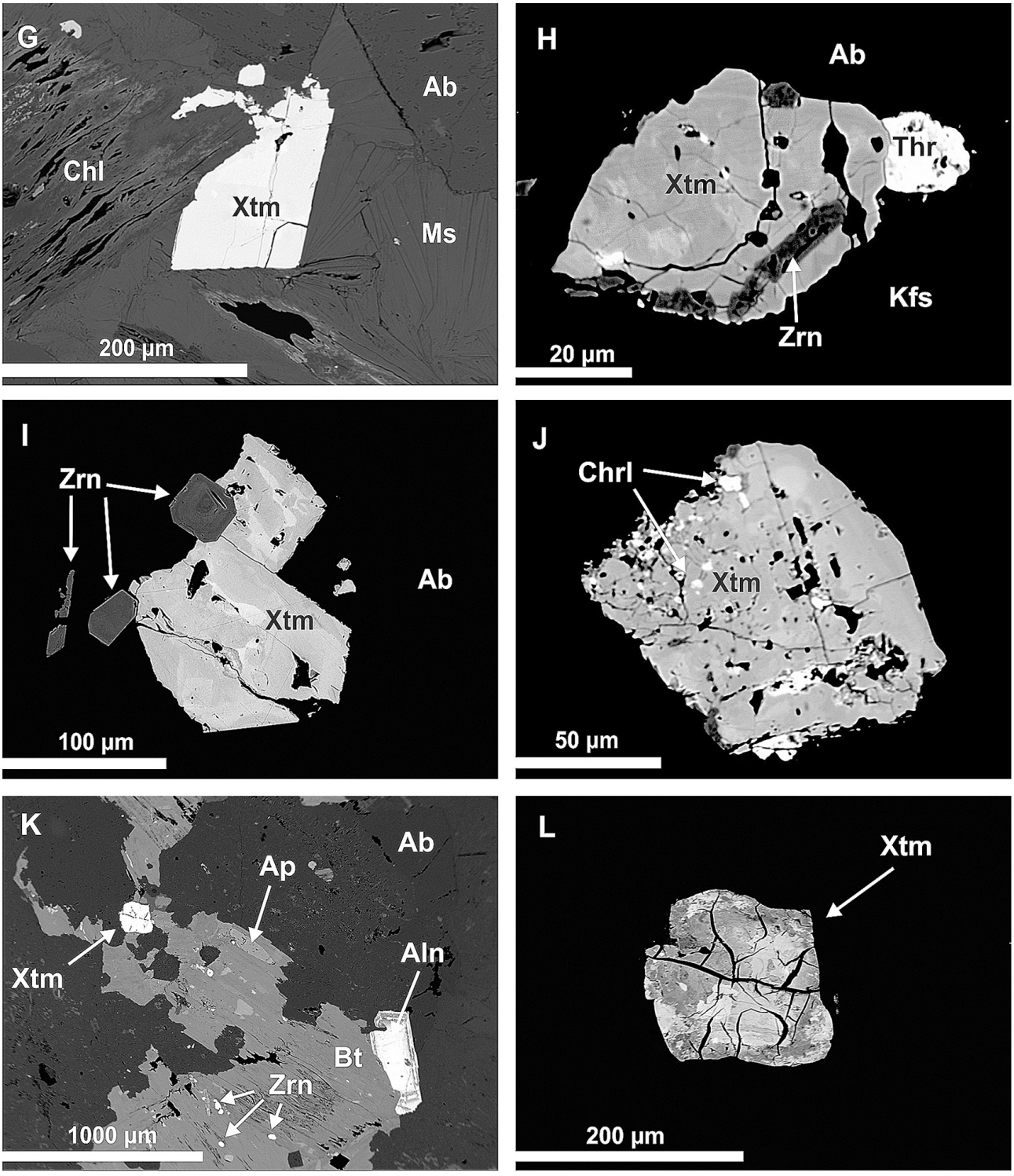

Fig. 2: continued – Back-scattered electron (BSE) images of xenotime-(Y) and associated minerals. G – Subhedral xenotime-(Y) – (Xtm) in association with partly chloritised (Chl) muscovite (Ms) and albite (Ab). Sample VEL-1 (granite). H – Heterogeneous crystal of xenotime-(Y) – (Xtm) with zircon inclusions (Zrn) and thorite (Thr). Rock-forming minerals are represented by albite (Ab) and K-feldspar (Kfs). Sample VEL-2F (granite). I – Typical isostructural relationship of accessory xenotime-(Y) – (Xtm) and zircon (Zrn) in albite (Ab). Xenotime-(Y) shows brighter Th, U-rich convolute zonation. Sample VEL-1 (granite). J – Large xenotime-(Y) crystal (Xtm) with secondary irregular zonation and porosity and numerous inclusions of cheralite (Chrl). Sample VEL-2F (granite). K – Accessory mineral assemblage of xenotime-(Y) – (Xtm), allanite-(Ce) – (Aln), fluorapatite (Ap) and zircon (Zrn) scattered in biotite (Bt) and albite (Ab). Sample VEL-9 (pegmatite). L – Detail of image K. Heterogeneous composition and secondary irregular zonation of xenotime-(Y) – (Xtm) with developed system of cracks and fissures. Sample VEL-9 (pegmatite). Mineral abbreviations are after Whitney & Evans (2010).

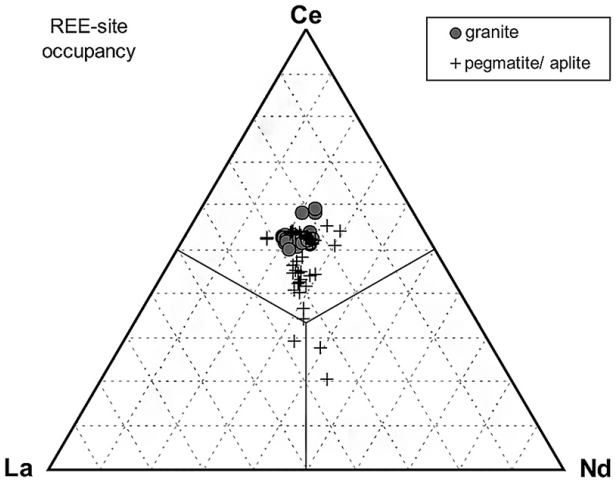

Fig. 3: Ternary diagram Ce–La–Nd showing MGM endmembers in parental granite and pegmatite/aplite with contrasting Ce, La and Nd distribution (atomic proportions).

Ce/La = 0.78 also occur in the pegmatite (Fig. 3, Tab. 3.). Yttrium concentration is relatively high (up to 12.7 wt.% Y_2O_3; 0.27 apfu Y) and there are also minor concentrations of heavy REE (HREE = Gd to Lu), with Gd the most significant (up to 4.9 wt.% Gd_2O_3; 0.06 apfu Gd).

Thorium and Ca contents vary greatly in MGM (0.53 to 34.9 wt.% ThO_2; up to 0.31 apfu Th; 0.1 to 10.7 wt.% CaO and 0.51 apfu Ca). These concentrations increase in MGM originating from pegmatite compared to that from granite, and MGM from pegmatite/aplite is generally richer in cheralite ($Ca_{0.5}Th_{0.5}PO_4$) and huttonite ($ThSiO_4$) components. Cheralite endmember occasionally occurs (Fig. 4A, 5), but is restricted to pegmatite/aplite only. The MGM from pegmatite has slightly increased F content up to 1.1 wt.% F, but the low totals suggest that the phases are most likely hydrated.

The MGM mole fractions are: X_{mnz} = 71 – 98; X_{hutt} = 0 – 17; X_{chrl} = 0 – 68 (Fig. 5). There is also depleted light REE (LREE

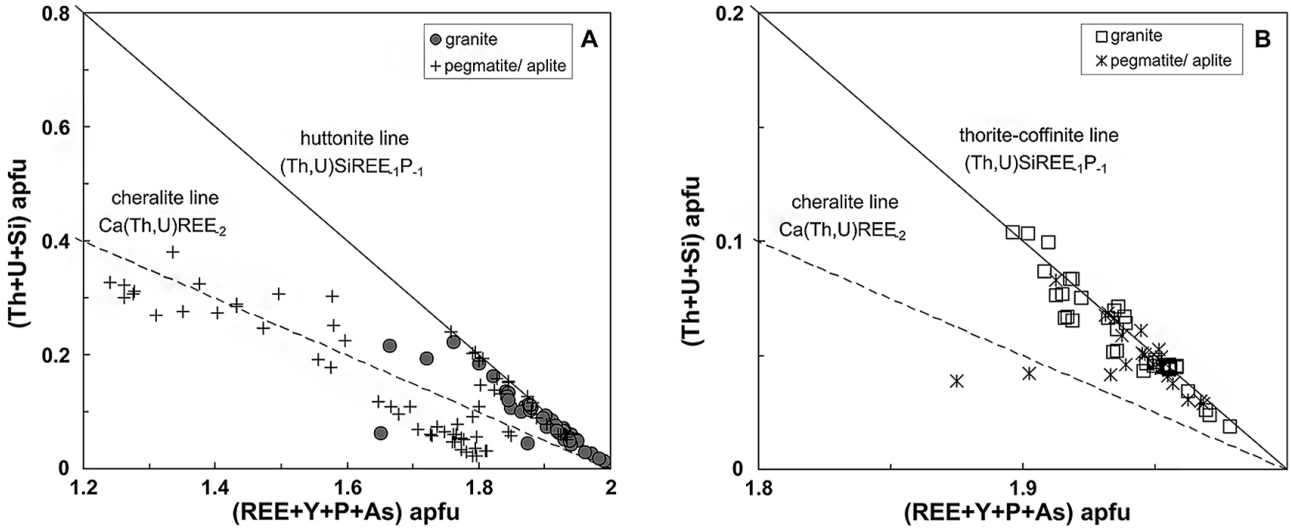

Fig. 4: Composition of accessory minerals in Th + U + Si vs. REE + Y + P + As substitution diagram (atomic proportions) with ideal cheralite and huttonite or thorite-coffinite substitution vectors (straight lines). A – MGM, B – xenotime-(Y).

4. RESULTS AND MINERAL COMPOSITION

4.1. Monazite-group minerals

The MGM form euhedral to anhedral solitary crystals and occasional aggregates, and their size mostly ranges from 20 to 200 μm (Fig. 2). The MGM has mostly oscillatory or irregular zoning visible on back-scattered electron (BSE) images and is generally associated with accessory xenotime-(Y) and zircon (Fig. 2B). It occasionally forms glomeroporphyric clusters (synneusis) scattered in the biotite and interstitial spaces (Fig. 2C) or euhedral crystals enclosed in feldspars (Fig. 2D). However, large fragmented MGM aggregates in close association with goyazite $SrAl_3(PO_4)_2(OH)_5 \cdot (H_2O)$, zircon and chlorite in feldspars are rarely present (Fig. 2F).

The investigated MGM are mostly Ce-dominant (up to 32.3 wt.% Ce_2O_3; 0.47 apfu Ce; Tab. 1). However, minor cheralitic monazite-(Nd) with Ce/Nd = 0.47 and monazite-(La) with

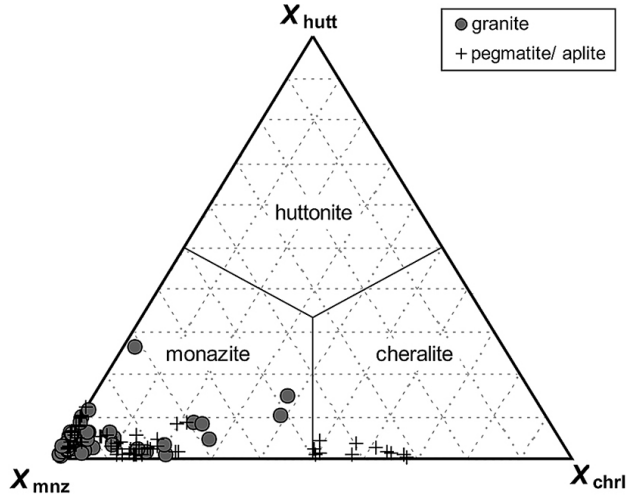

Fig. 5: Ternary diagram of MGM mole fractions (X_{mnz} = monazite, X_{hutt} = huttonite, X_{chrl} = cheralite) in parental granite and pegmatite/aplite with contrasting mole fractions distribution.

= La to Sm) content at the expense of other minor elements, mostly Th and Ca. The Ce deficiency relative to other LREE in the pegmatite/aplite is evident in the REE mineral/chondrite normalised patterns (Fig. 6). The compositional X-ray mapping shows that monazite-(Ce) crystal from the host granite has relatively homogeneous REE distribution and Th enrichment in marginal areas (Fig. 7). Other trace elements (As, S, Sr, Ba and Cl) are generally very low or below EPMA detection limit (Tab. 3).

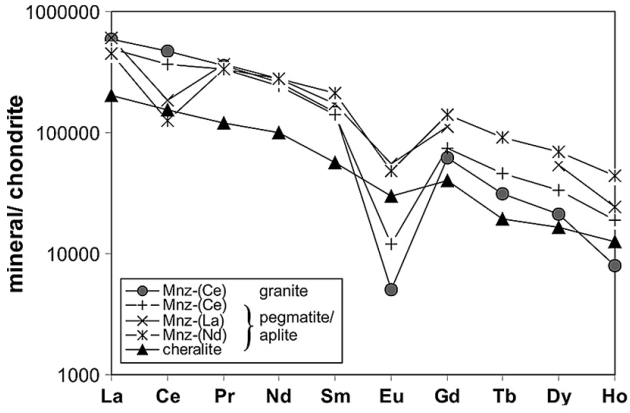

Fig. 6: Chondrite-normalised patterns of selected REE in MGM from parental granite and pegmatite/aplite. Normalised values after Barrat et al. (2012).

4.2. Xenotime-(Y)

Accessory xenotime-(Y) is the main carrier of HREE in the VGM but it has relatively less abundance than MGM and occurs as anhedral to subhedral crystals up to 200 μm in size. Xenotime-(Y) is associated with zircon, cheralite, allanite-(Ce) and fluorapatite (Fig. 2), and most crystals have numerous tiny inclusions of Th-silicate (thorite?) or Ca-Th-phosphate (cheralite) and show irregular zoning reflecting the variable REE/Th-Ca ratio (Fig. 2H, J). There are also irregularly shaped areas within the crystals and forming aureoles around the Th-Ca inclusions. The darker areas are richer in REE and these record relative depletion of Th and partly also U. Finally, the secondary zone development

Table 3: Representative compositions of EPMA of MGM (wt. %).

Sample	VEL-1	VEL-2F	VEL-2G	VEL-3B	VEL-8A	VEL-8C	VEL-9	VEL-9A	VEL-9A	VEL-9A
End member	Mnz-(Ce)	Mnz-(Ce)	Mnz-(Ce)	Mnz-(Ce)	Mnz-(Ce)	Mnz-(Ce)	Mnz-(Nd)	Mnz-(La)	Chrl	Chrl
SO_3	0.02	0.01	0.02	0.03	0.02	0.02	0.24	0.18	0.08	0.21
P_2O_5	28.94	26.09	26.95	25.11	27.80	27.43	28.09	28.98	27.75	28.56
As_2O_5	0.00	0.00	0.00	0.01	0.00	0.00	0.00	0.15	0.20	0.00
SiO_2	0.61	2.88	2.51	2.99	1.46	2.55	0.48	1.54	2.18	0.67
ThO_2	4.41	11.21	9.86	12.28	9.65	5.74	11.07	4.52	18.57	28.91
UO_2	0.05	0.44	0.40	0.29	0.17	0.75	0.21	0.00	0.18	0.20
Al_2O_3	0.00	0.00	0.14	0.00	0.00	0.00	0.35	1.05	0.00	0.00
Y_2O_3	2.03	3.79	3.04	0.90	0.70	3.11	5.26	4.57	3.43	2.78
La_2O_3	13.74	10.34	11.57	12.81	16.90	7.90	10.63	14.14	8.66	7.06
Ce_2O_3	28.75	22.81	25.91	27.52	28.80	26.26	8.96	11.03	18.01	12.81
Pr_2O_3	3.31	2.88	3.17	3.20	2.89	3.83	3.08	3.37	1.90	1.60
Nd_2O_3	12.15	11.50	12.13	11.24	8.96	14.67	12.86	12.87	8.39	5.40
Sm_2O_3	2.30	2.63	2.61	1.73	1.11	3.19	3.11	2.66	1.77	0.57
Eu_2O_3	0.06	0.00	0.01	0.03	0.06	0.00	0.31	0.32	0.00	0.18
Gd_2O_3	1.58	1.80	2.01	0.57	0.46	1.75	2.38	2.32	1.74	1.02
Tb_2O_3	0.14	0.23	0.20	0.05	0.07	0.19	0.20	0.00	0.21	0.16
Dy_2O_3	0.70	0.94	0.89	0.23	0.18	0.96	1.36	1.36	0.92	0.54
Ho_2O_3	0.05	0.15	0.13	0.00	0.00	0.08	0.11	0.14	0.11	0.08
Er_2O_3	0.46	0.62	0.51	0.35	0.25	0.34	0.63	0.38	0.38	0.50
Tm_2O_3	0.11	0.12	0.11	0.09	0.01	0.06	0.12	0.27	0.00	0.24
Yb_2O_3	0.16	0.22	0.15	0.14	0.13	0.20	0.35	0.31	0.00	0.33
Lu_2O_3	0.08	0.07	0.13	0.10	0.15	0.08	0.11	0.36	0.00	0.25
CaO	0.47	0.35	0.19	0.09	1.03	0.11	4.20	3.71	4.02	6.82
SrO	0.01	0.00	0.03	0.00	0.01	0.01	0.08	0.00	0.00	0.18
FeO total	0.00	0.02	0.06	0.00	0.82	0.43	2.09	0.00	0.90	0.63
PbO	0.06	0.13	0.13	0.16	0.13	0.10	1.63	1.47	0.08	0.11
F	0.00	0.00	0.00	0.00	0.00	0.00	0.44	1.12	0.00	0.00
Total	**100.17**	**99.24**	**102.86**	**99.90**	**101.76**	**99.76**	**98.36**	**96.82**	**99.47**	**99.82**

Table 3: continued - Representative compositions of EPMA of MGM (apfu).

Sample	VEL-1	VEL-2F	VEL-2G	VEL-3B	VEL-8A	VEL-8C	VEL-9	VEL-9A	VEL-9A	VEL-9A
End member	Mnz-(Ce)	Mnz-(Ce)	Mnz-(Ce)	Mnz-(Ce)	Mnz-(Ce)	Mnz-(Ce)	Mnz-(Nd)	Mnz-(La)	Chrl	Chrl
S^{6+}	0.001	0.000	0.001	0.001	0.001	0.001	0.007	0.005	0.002	0.006
P^{5+}	0.968	0.891	0.895	0.873	0.926	0.915	0.915	0.904	0.914	0.943
As^{5+}	0.000	0.000	0.000	0.000	0.000	0.000	0.000	0.003	0.004	0.000
Si^{4+}	0.024	0.116	0.098	0.123	0.058	0.100	0.019	0.057	0.085	0.026
Th^{4+}	0.040	0.103	0.088	0.115	0.086	0.051	0.097	0.038	0.165	0.256
U^{4+}	0.000	0.004	0.003	0.003	0.001	0.007	0.002	0.000	0.002	0.002
Al^{3+}	0.000	0.000	0.006	0.000	0.000	0.000	0.016	0.046	0.000	0.000
Y^{3+}	0.043	0.081	0.064	0.020	0.015	0.065	0.108	0.090	0.071	0.058
La^{3+}	0.200	0.154	0.167	0.194	0.245	0.115	0.151	0.192	0.124	0.102
Ce^{3+}	0.416	0.337	0.372	0.414	0.415	0.379	0.126	0.149	0.257	0.183
Pr^{3+}	0.048	0.042	0.045	0.048	0.041	0.055	0.043	0.045	0.027	0.023
Nd^{3+}	0.172	0.166	0.170	0.165	0.126	0.207	0.177	0.169	0.117	0.075
Sm^{3+}	0.031	0.037	0.035	0.025	0.015	0.043	0.041	0.034	0.024	0.008
Eu^{3+}	0.001	0.000	0.000	0.000	0.001	0.000	0.004	0.004	0.000	0.002
Gd^{3+}	0.021	0.024	0.026	0.008	0.006	0.023	0.030	0.028	0.022	0.013
Tb^{3+}	0.002	0.003	0.003	0.001	0.001	0.002	0.003	0.000	0.003	0.002
Dy^{3+}	0.009	0.012	0.011	0.003	0.002	0.012	0.017	0.016	0.011	0.007
Ho^{3+}	0.001	0.002	0.002	0.000	0.000	0.001	0.001	0.002	0.001	0.001
Er^{3+}	0.006	0.008	0.006	0.005	0.003	0.004	0.008	0.004	0.005	0.006
Tm^{3+}	0.001	0.002	0.001	0.001	0.000	0.001	0.001	0.003	0.000	0.003
Yb^{3+}	0.002	0.003	0.002	0.002	0.002	0.002	0.004	0.003	0.000	0.004
Lu^{3+}	0.001	0.001	0.002	0.001	0.002	0.001	0.001	0.004	0.000	0.003
Ca^{2+}	0.020	0.015	0.008	0.004	0.043	0.005	0.173	0.147	0.168	0.285
Sr^{2+}	0.000	0.000	0.001	0.000	0.000	0.000	0.002	0.000	0.000	0.004
Fe^{2+}	0.000	0.001	0.002	0.000	0.027	0.014	0.067	0.000	0.029	0.020
Pb^{2+}	0.001	0.001	0.001	0.002	0.001	0.001	0.017	0.015	0.001	0.001
Position *X*	0.993	1.008	0.994	0.997	0.984	1.016	0.940	0.969	1.005	0.975
Position *A*	1.013	0.996	1.016	1.008	1.034	0.990	1.089	0.989	1.026	1.058
Total	**2.005**	**2.004**	**2.010**	**2.005**	**2.018**	**2.006**	**2.030**	**1.958**	**2.032**	**2.033**

indicates xenotime-(Y) alteration and secondary thorite and cheralite formation (Fig. 2G, J).

In addition to Y (up to 46.7 wt.% Y_2O_3; 0.80 apfu Y), xenotime-(Y) also has elevated HREE concentrations. These are principally Dy (up to 7.0 wt.% Dy_2O_3; 0.08 apfu Dy) and Yb (up to 5.8 of wt.% Yb_2O_3; 0.06 apfu Yb). The LREE are not readily incorporated into the xenotime-(Y) structure, and consequently have max. value of only 2.65 wt.% $LREE_2O_3$ (0.03 apfu LREE).

The actinide elements (Th, U) vary in concentration but Th > U (up to 4.4 wt.% ThO_2; 0.034 apfu Th and up to 2.0 wt % UO_2; 0.02 apfu U; Fig. 8, Tab. 4). There is also positive correlation between Th+U+Si and REE+P (apfu), and this indicates coupled substitution corresponding to the thorite and coffinite $(Th+U)SiREE_{-1}P_{-1}$ substitution vector (Fig 4B).

The chemical composition of xenotime-(Y) and normalised REE patterns have no significant difference in parental granite and pegmatite/aplite. Both REE patterns show a weakly-developed M-type tetrad effect in HREE (granite: T3 = 1.22, T4 = 0.98, combined T3-4 = 1.1; pegmatite/aplite: T3 = 1.27, T4 = 1.04, combined T3-4 = 1.15; calculation according to Irber (1999), see Fig. 9. In addition, X-ray elemental mapping of xenotime-(Y) crystal from the parental granite reveals relatively homogeneous distribution of REE, and Ca, Th and Si distribution suggests the presence of tiny cheralite inclusions (Fig. 10). Other trace elements (As and S) are generally very low or below the EPMA detection limit (Tab. 4.).

4.3. Monazite-(Ce) and xenotime-(Y) in-situ chemical dating

Non-stoichiometric and altered Th-Ca-rich MGM have low totals and they were therefore omitted from the age calculation. The applied dating method gave the following ages: 289 ± 2.9 Ma (monazite, n = 62, MSWD: 3.22; Fig. 11, Tab. 5.) and 266 ± 5.2 Ma (xenotime, n = 44, MSWD: 1.4; Fig. 12, Tab. 6.). The data also elucidated systematic primary Permian (Cisuralian) magmatic age for granitic intrusion emplacement

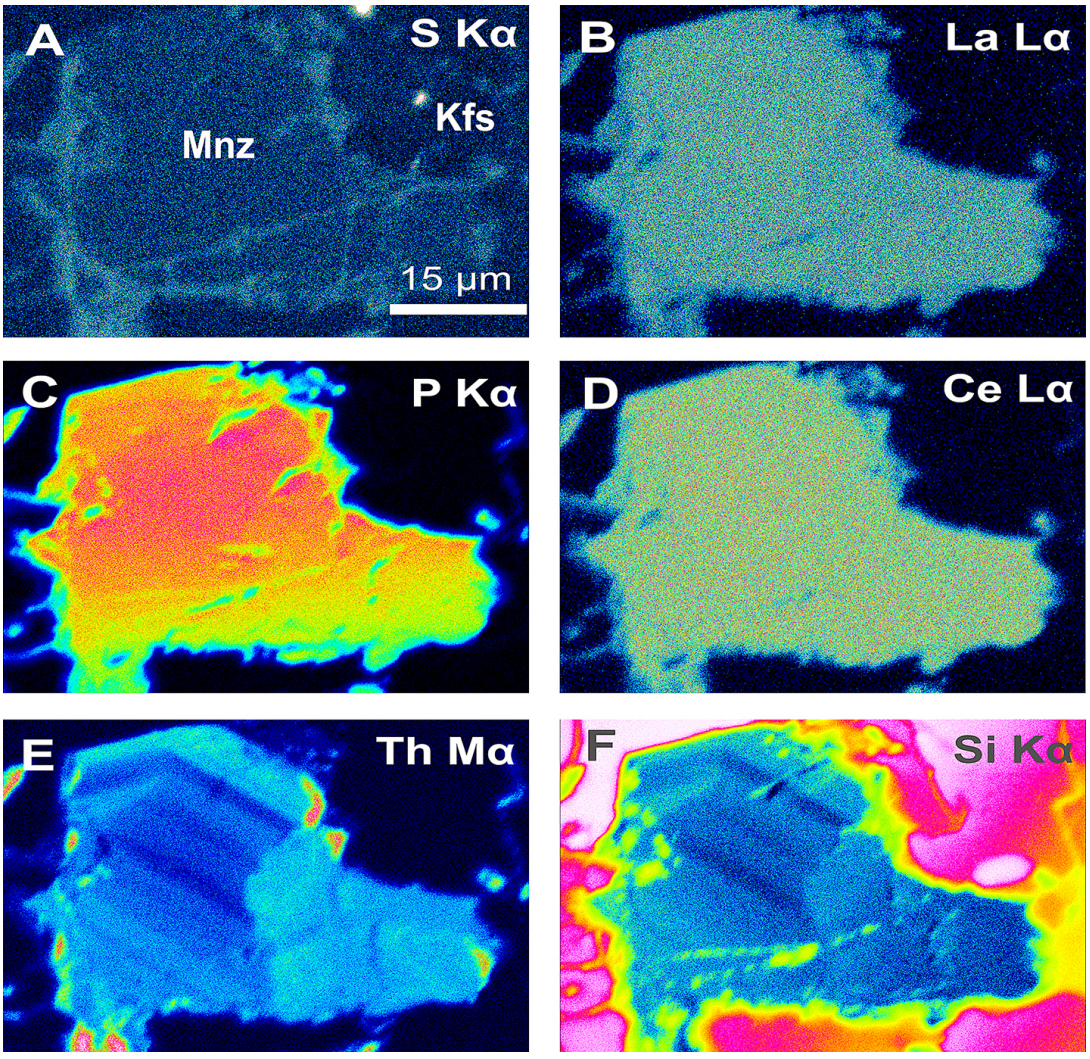

Fig. 7: False colour X-ray mapping showing the distribution of chemical elements in MGM. False colours: blue – very low, green – low, yellow – medium, orange – high, red – very high.

and Permian (Guadalupian) crystallization of the apparently younger xenotime-(Y). Moreover, the sporadic occurrence of 670 – 640 Ma old monazite-(Ce) domains in the Velence

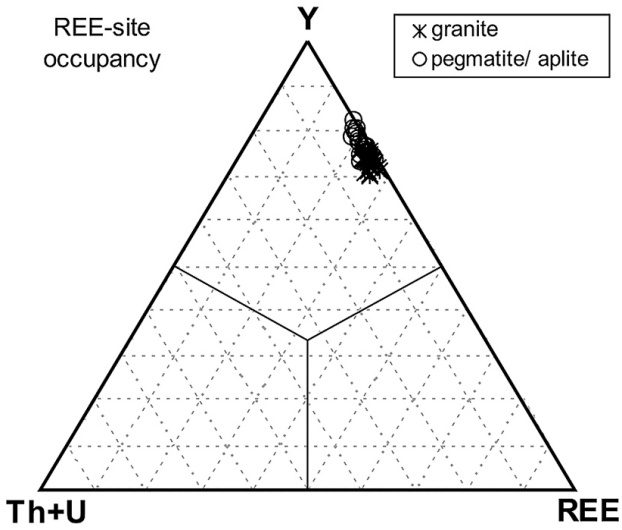

Fig. 8: Ternary diagram Y–REE–(Th+U) showing xenotime-(Y) composition in parental granite and pegmatite/aplite.

granite was detected in all dated samples (n = 11). However, the detailed comparative study of EPMA in-situ chemical dating spots shows no age differences between MGM and xenotime-(Y) populations from parental granite and those from pegmatite/aplite.

5. DISCUSSION AND CONCLUSIONS

5.1. Monazite-group minerals and xenotime-(Y) composition and typomorphic distribution

Monazite-(Ce) and xenotime-(Y) are important accessory REE-bearing minerals and reliable petrogenetic indicators of granitic rock evolutionary history. In particular, monazite-(Ce) is the most common accessory LREE-rich mineral phase of peraluminous and low-Ca granitic suites, commonly with S-type, or highly evolved I-type affinity (e.g., Broska & Uher, 1991; Bea, 1996; Förster, 1998; Kelts et al., 2008; Petrík & Konečný, 2009; Broska et al., 2012[b]; Uher et al., 2014). REE phosphates are almost absent in hypersolvus A-type granites, but they sporadically occur in the subsolvus type with allanite-(Ce) the dominant REE-bearing phase (e.g., Uher & Broska,

Table 4: Representative compositions of EPMA of xenotime-(Y) (wt.%).

Sample	VEL-1	VEL-1	VEL-1	VEL-2F	VEL-2F	VEL-6C	VEL-8A	VEL-8B	VEL-8B	VEL-8C	VEL-10
End member	Xtm	Xtm	Xtm	Xtm	Xtm	Xtm	Xtm	Xtm	Xtm	Xtm	Xtm
SO_3	0.01	0.03	0.01	0.02	0.02	0.12	0.00	0.02	0.01	0.01	0.02
P_2O_5	33.83	33.24	32.37	34.64	34.63	34.98	32.95	33.72	33.18	34.75	32.61
As_2O_5	0.00	0.00	0.00	0.01	0.03	0.10	0.07	0.10	0.03	0.06	0.00
SiO_2	1.05	1.60	1.47	0.74	0.93	1.21	1.63	1.53	4.15	0.71	1.18
ThO_2	0.79	2.56	2.39	1.10	0.84	0.16	2.16	1.09	0.19	0.35	0.50
UO_2	0.84	1.63	1.76	1.23	1.78	0.15	1.49	1.06	0.73	0.49	1.03
Al_2O_3	0.00	0.00	0.00	0.00	0.00	0.00	0.00	0.00	0.79	0.00	0.00
Y_2O_3	40.17	38.16	37.65	39.67	39.66	46.62	41.21	43.21	38.81	42.62	39.43
La_2O_3	0.00	0.00	0.00	0.00	0.00	0.00	0.00	0.00	0.00	0.00	0.00
Ce_2O_3	0.06	0.14	0.12	0.08	0.11	0.11	0.09	0.07	0.12	0.10	0.07
Pr_2O_3	0.21	0.24	0.17	0.21	0.18	0.14	0.16	0.14	0.13	0.17	0.14
Nd_2O_3	0.38	0.69	0.72	0.37	0.46	0.12	0.25	0.34	0.54	0.20	0.53
Sm_2O_3	1.13	1.58	1.50	0.73	0.73	0.54	0.78	0.75	1.55	0.74	1.68
Eu_2O_3	0.04	0.00	0.13	0.00	0.00	0.09	0.00	0.00	0.00	0.00	0.09
Gd_2O_3	3.66	4.34	4.28	2.48	2.46	2.46	2.83	2.36	4.08	2.67	4.70
Tb_2O_3	0.77	0.90	0.85	0.60	0.56	0.66	0.69	0.57	0.91	0.66	0.97
Dy_2O_3	6.10	6.42	6.31	4.97	5.11	5.20	5.48	4.88	6.02	5.12	6.85
Ho_2O_3	1.08	1.04	1.05	0.91	0.99	0.76	1.04	0.94	0.98	1.05	1.11
Er_2O_3	4.37	4.11	4.18	4.30	4.36	2.93	4.04	4.20	3.82	4.48	4.48
Tm_2O_3	0.72	0.62	0.64	0.79	0.78	0.45	0.65	0.66	0.63	0.77	0.69
Yb_2O_3	3.96	3.28	3.44	5.79	5.17	2.50	3.99	3.76	3.36	4.62	3.82
Lu_2O_3	0.60	0.47	0.56	1.07	0.84	0.41	0.48	0.49	0.35	0.54	0.63
CaO	0.07	0.11	0.03	0.02	0.10	0.17	0.01	0.03	0.16	0.05	0.01
FeO total	0.03	0.01	0.01	0.00	0.04	1.37	0.57	0.23	0.08	0.07	0.64
PbO	0.00	0.09	0.09	0.07	0.08	0.00	0.09	0.05	0.02	0.02	0.01
Total	**99.88**	**101.26**	**99.73**	**99.81**	**99.85**	**101.22**	**100.65**	**100.21**	**100.63**	**100.24**	**101.20**

1996; Broska et al., 2012[b]). This typomorphic distribution of accessory phases is most likely controlled by P, LREE and Ca content in melt and by magmatic differentiation and redox conditions.

The accessory mineral assemblage of major allanite-(Ce) + ilmenite ± magnetite in the Velence granite indicates intermediate oxygen fugacity (fO_2) values (cf. Uher & Broska, 1996), and the relatively high activity of Ca stabilises allanite-(Ce) while

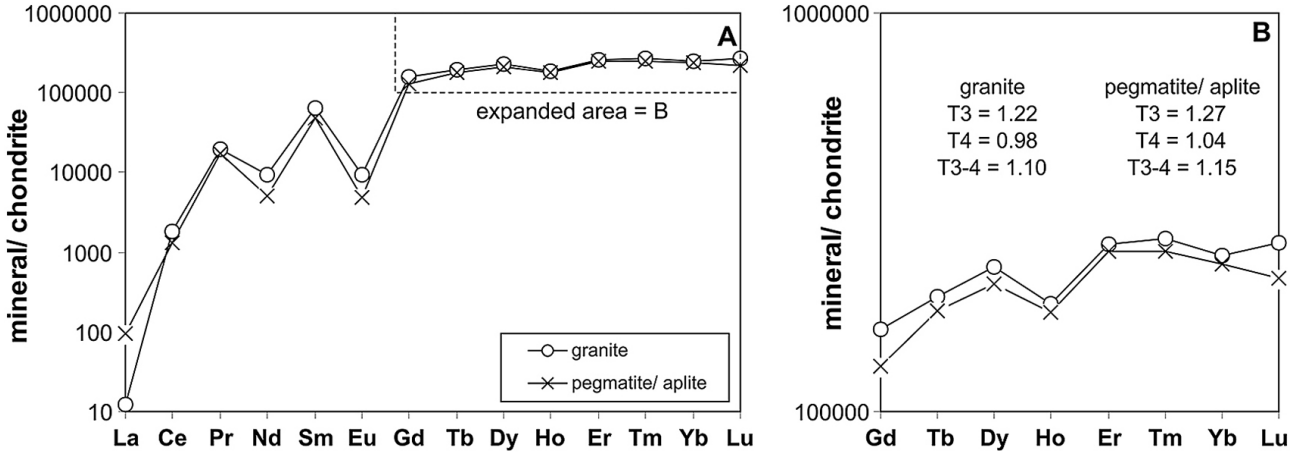

Fig. 9: Chondrite-normalised REE patterns A – in xenotime-(Y) from parental granite and pegmatite/aplite, B – Detail of HREE tetrad effect. Normalised values after Barrat et al. (2012).

Table 4: continued - Representative compositions of EPMA of xenotime-(Y) (apfu).

End member	Xtm	Xtm	Xtm	Xtm	Xtm	Xtm	Xtm	Xtm	Xtm	Xtm	Xtm
S^{6+}	0.000	0.001	0.000	0.001	0.000	0.003	0.000	0.001	0.000	0.000	0.000
P^{5+}	0.973	0.956	0.953	0.992	0.988	0.959	0.946	0.955	0.917	0.983	0.947
As^{5+}	0.000	0.000	0.000	0.000	0.001	0.002	0.001	0.002	0.001	0.001	0.000
Si^{4+}	0.036	0.054	0.051	0.025	0.031	0.039	0.055	0.051	0.136	0.024	0.040
Th^{4+}	0.006	0.020	0.019	0.008	0.006	0.001	0.017	0.008	0.001	0.003	0.004
U^{4+}	0.006	0.012	0.014	0.009	0.013	0.001	0.011	0.008	0.005	0.004	0.008
Al^{3+}	0.000	0.000	0.000	0.000	0.000	0.000	0.000	0.000	0.030	0.000	0.000
Y^{3+}	0.726	0.690	0.696	0.714	0.712	0.803	0.744	0.770	0.675	0.758	0.720
La^{3+}	0.000	0.000	0.000	0.000	0.000	0.000	0.000	0.000	0.000	0.000	0.000
Ce^{3+}	0.001	0.002	0.002	0.001	0.001	0.001	0.001	0.001	0.001	0.001	0.001
Pr^{3+}	0.003	0.003	0.002	0.003	0.002	0.002	0.002	0.002	0.002	0.002	0.002
Nd^{3+}	0.005	0.008	0.009	0.004	0.006	0.001	0.003	0.004	0.006	0.002	0.006
Sm^{3+}	0.013	0.019	0.018	0.009	0.008	0.006	0.009	0.009	0.017	0.009	0.020
Eu^{3+}	0.001	0.000	0.002	0.000	0.000	0.001	0.000	0.000	0.000	0.000	0.001
Gd^{3+}	0.041	0.049	0.049	0.028	0.028	0.026	0.032	0.026	0.044	0.030	0.053
Tb^{3+}	0.009	0.010	0.010	0.007	0.006	0.007	0.008	0.006	0.010	0.007	0.011
Dy^{3+}	0.067	0.070	0.071	0.054	0.056	0.054	0.060	0.053	0.063	0.055	0.076
Ho^{3+}	0.012	0.011	0.012	0.010	0.011	0.008	0.011	0.010	0.010	0.011	0.012
Er^{3+}	0.047	0.044	0.046	0.046	0.046	0.030	0.043	0.044	0.039	0.047	0.048
Tm^{3+}	0.008	0.007	0.007	0.008	0.008	0.005	0.007	0.007	0.006	0.008	0.007
Yb^{3+}	0.041	0.034	0.036	0.060	0.053	0.025	0.041	0.038	0.033	0.047	0.040
Lu^{3+}	0.006	0.005	0.006	0.011	0.009	0.004	0.005	0.005	0.003	0.005	0.007
Ca^{2+}	0.003	0.004	0.001	0.001	0.003	0.006	0.000	0.001	0.006	0.002	0.000
Fe^{2+}	0.001	0.000	0.000	0.000	0.001	0.037	0.016	0.007	0.002	0.002	0.018
Pb^{2+}	0.000	0.001	0.001	0.001	0.001	0.000	0.001	0.000	0.000	0.000	0.000
Position *X*	1.009	1.012	1.004	1.018	1.021	1.002	1.002	1.009	1.054	1.008	0.988
Position *A*	0.994	0.988	1.000	0.973	0.970	1.018	1.011	0.999	0.956	0.993	1.035
Total	**2.003**	**2.000**	**2.004**	**1.990**	**1.991**	**2.020**	**2.013**	**2.008**	**2.010**	**2.001**	**2.023**

monazite-(Ce) occurrence indicates relatively low Ca activity (Lee & Dodge, 1964; Lee & Silver, 1964; Lee & Bastron, 1967; Snetsinger, 1967; Cuney & Friedrich, 1987; Parrish, 1990; Casillas et al., 1995; Broska et al., 2006). Although allanite-(Ce) is present to the exclusion of monazite-(Ce) in rocks that contain more than about 2.0 wt.% CaO and only monazite-(Ce) is present in rocks with less than 0.7% CaO, both allanite-(Ce) and monazite-(Ce) are present at intermediate CaO values (Lee & Dodge, 1964; Lee & Bastron, 1967).

In contrast, monazite-(Ce) composition is normally almost the pure REE endmember when it is present in A-type granitoids, especially in hypersolvus conditions. This allows only limited $ThSiREE_{-1}P_{-1}$ huttonite entry and/or negligible $Ca(Th,U)REE_{-2}$ cheralite substitution. This appears to be a characteristic feature of hypersolvus A-type granitoid rocks where Ca is lacking in the bulk-rock (0.05 wt.% CaO) - (Ondrejka et al., 2007).

The MGM from the subsolvus Velence granitic rock samples are relatively rich in Th (≤ 10.6 wt.% ThO_2). This is most likely related to higher Th content in monazite-(Ce) which crystallized at higher temperatures (Broska et al., 2000), and it accords with the hot and dry origin of A-type granitic rocks (cf. Whalen et al., 1987). In contrast, Th-enrichment is more developed in the pegmatite/aplite varieties and, combined with Ca, it stabilises cheralitic monazite and cheralite as the relatively common accessory phase (Gramaccioli & Segalstad, 1978; Bea, 1996; Förster, 1998; Pérez-Soba et al., 2014; Uher et al., 2014). Here, Ca-rich MGM most likely crystalised as an early magmatic or orthomagmatic phase before Ca was consumed by formation of primary allanite-(Ce) as the dominant REE accessory mineral.

While MGM is typically Ce-dominant in parental granite, there are some instances of La or Nd endmember dominance with Ce/La = 0.78 and Ce/Nd = 0.47. These monazite-(La) and monazite-(Nd) endmembers and enrichment trends towards La ≈ Nd > Ce are only observed in MGM from the pegmatite samples. Here, negative Ce anomaly is recognised and such Ce deficiency relative to La and Nd cannot be therefore explained by selective and differential REE complexing in the granite-to-pegmatite solidification sequence where the tetrad effect on LREE is usually developed (e.g., Masau et al., 2002). Cerium anomalies in REE accessory minerals commonly develop in highly oxidised and fluid-rich environments, which causes fractionation of REE

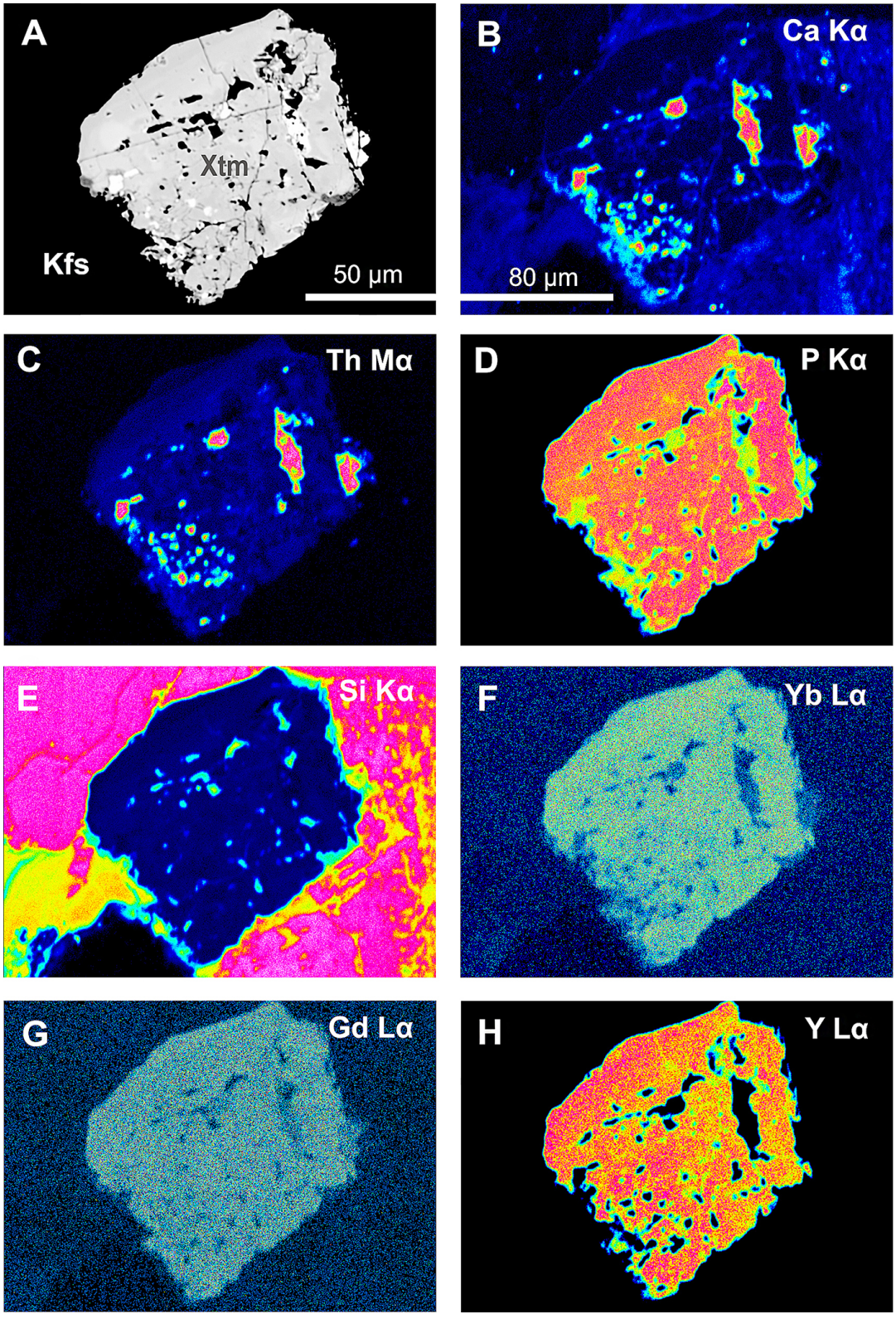

Fig. 10: False colour X-ray mapping showing the distribution of chemical elements in xenotime-(Y). False colours: blue – very low, green – low, yellow – medium, orange – high, red – very high.

by oxidation of Ce^{3+} to Ce^{4+} (Fisher & Meyrowitz, 1962; Banfield & Eggleton, 1989; Braun et al., 1990; Demartin et al., 1991[b]; Gieré & Sorensen, 2004; Mayer et al., 2014; MacDonald et al., 2015; Bagiński et al., 2016; Ondrejka et al., 2018). In contrast, weakly developed tetrad effect in T3 (Gd to Ho) and T4 (Er to Lu) tetrads in xenotime-(Y) is probably an inherited geochemical signature of A-type parental melt (rich in F), since it occurs also in xenotime-(Y) from granite and gradually evolves during the progressive crystallization of the pegmatite derivates. The mechanism of formation of the tetrad effect remains still unclear, but it is obviously connected to F-controlled complexing in highly evolved ligand-rich environments (e.g., Irber, 1999;

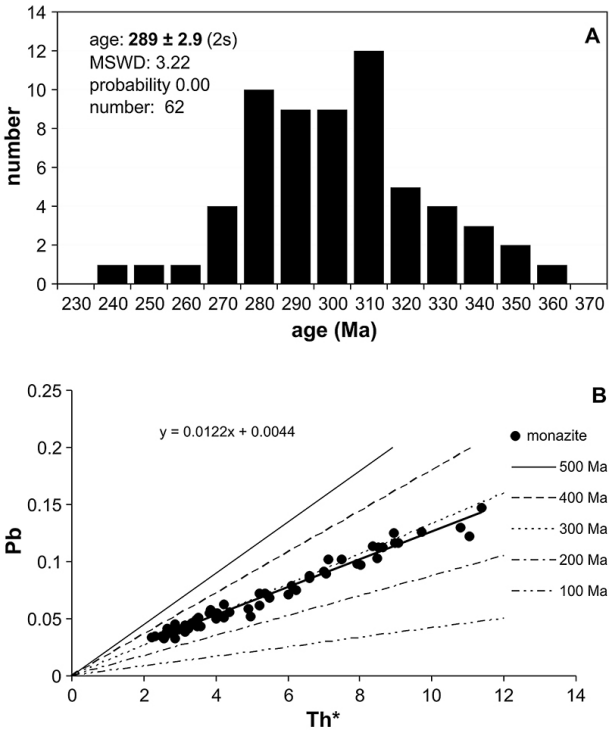

Fig. 11: Th–U–total Pb EPMA dating. A: histogram, B: isochron diagram of MGM ages from Velence. Pb values are in wt. %, Th* = Th + 3.15*U wt. %.

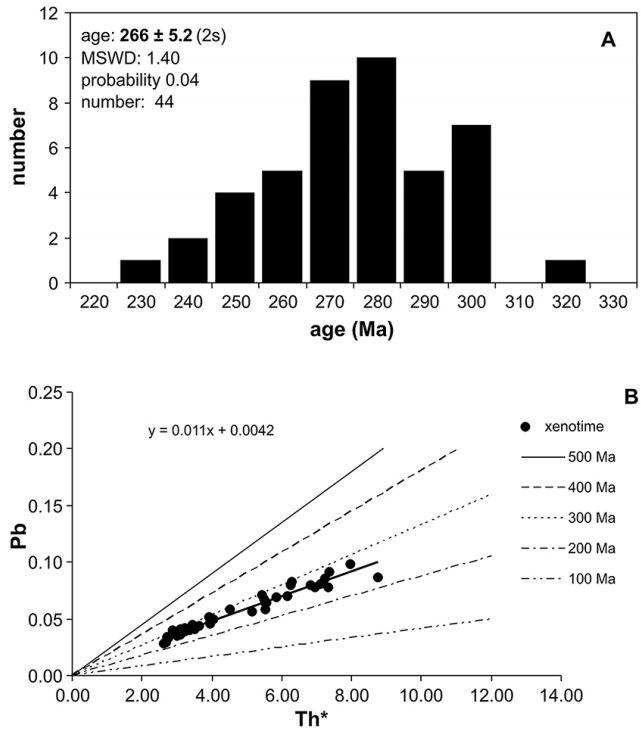

Fig. 12: Th–U–total Pb EPMA dating. A: histogram, B: isochron diagram of xenotime-(Y) ages from Velence. Pb values are in wt. %, Th* = Th + 3.15*U wt. %.

Masau et al., 2002; Veksler et al., 2005; Badanina et al., 2006; Čopjaková et al., 2015).

Although, the concentration of fluorine in MGM from parental granite is negligible and often zero, an increased F content (0.3 – 1.2 wt.%) was observed in MGM from pegmatite. This suggests that F was preferentially consumed by simultaneous crystallization of primary fluorapatite (cf. Broska, 2001). Some large Ca-Th-rich crystals with low totals in pegmatite most likely represent altered(?) cheralitic MGM or brockitic rhabdophane group minerals (RGM) where elevated Y and HREE anomaly are typical compositional features (Nagy et al., 2002; Krenn & Finger, 2007; Ondrejka et al., 2018) and are in contrast with structural adjustments to the different sizes of REE atoms in monazite-(Ce) and xenotime-(Y) dimorphs (Ni et al., 1995). These brockite- and tristramite-rich supergene RGM with euhedral hexagonal symmetry associated with alunite supergroup minerals, clay minerals and goethite are also present in the Velence microgranite (Ondrejka et al., 2018).

While monazite-(Ce) from parental granite remains relatively unaffected by later post-magmatic-hydrothermal alteration, xenotime-(Y) was partly altered. This takes the form of remobilised $CaTh(PO_4)_2$ and particularly $(Th, U)SiO_4$ enrichment of a xenotime-(Y) portion via the coupled substitution reactions $Ca^{2+}+Th^{4+} \leftrightarrow 2REE^{3+}$, and $(Th, U)^{4+}+Si^{4+} \leftrightarrow REE^{3+}+P^{5+}$ respectively (e.g., Harlov, 2010). The partial chemical alteration of xenotime-(Y) caused irregular patchy zoning and subsequent growth of numerous tiny cheralite and thorite inclusions close to altered areas (Fig. 2H, J), and this can be explained by the occurrence of a younger dissolution-reprecipitation process (e.g., Harlov et al., 2005; Putnis et al., 2007; Ondrejka et al., 2016). This required in-situ fluid-aided element redistribution; especially of Ca, Th, and U. A very similar dissolution-reprecipitation microtexture of thorite and/or uraninite inclusions in xenotime-(Y) and associated monazite-(Ce) has been described in granitic pegmatites in the Hidra anorthosite massif in Norway (Hetherington & Harlov, 2008) and in granitic orthogneisses in the Veporic pre-Alpine-basement, Western Carpathians, Slovakia (Ondrejka et al., 2016). Textural and crystal-chemical evidence therefore suggests that cheralite and thorite inclusions occurred from fluid-mineral interaction in a closed chemical system, where all components necessary for nucleation and growth of the inclusions were already present in the host xenotime-(Y) – (Hetherington & Harlov, 2008). This also suggest the relatively low mobility of actinides during dissolution-reprecipitation because significant amounts were unable to leave the xenotime-(Y) crystal (Ondrejka et al., 2012, 2016).

5.2. Monazite and xenotime formation and age

The presented 289 ± 2.9 Ma EPMA monazite in-situ chemical age is within error of the 283 ± 5 Ma; in-situ U–Pb SHRIMP zircon age (Uher & Ondrejka, 2009) from the same granitic rocks and indicates an Early Permian (Cisuralian) magmatic event. These ages are supported by previously published 280 ± 7 Ma Rb–Sr whole-rock dating (Buda, 1985) and 271–291 Ma K–Ar, and Rb–Sr biotite dating (Horváth et al., 2004). These suggest older Velence granite massif age than similar A-type granite plutonism in the Western Carpathian region (Turčok, Hrončok, Upohlav: 262–267 Ma). This significant time gap of approximately 20 Ma

Table 5: Analytical data and ages of monazite-(Ce) from the investigated samples.

Sample	Th	U	Pb	Y	Age	Age	Sample	Th	U	Pb	Y	Age	Age
	wt.%	wt.%	wt.%	wt.%	(Ma)	2σ		wt.%	wt.%	wt.%	wt.%	(Ma)	2σ
VEL-1	5.340	0.050	0.069	0.879	280	23.1	VEL-2	2.421	0.167	0.041	1.897	309	42.7
VEL-1	3.660	0.059	0.057	1.039	333	32.1	VEL-2	2.633	0.160	0.039	1.906	275	40.2
VEL-1	3.114	0.041	0.041	0.963	283	37.6	VEL-2	1.913	0.118	0.034	1.713	334	54.9
VEL-1	2.370	0.037	0.034	1.154	309	49.0	VEL-2	3.419	0.245	0.063	2.193	333	30.7
VEL-1	3.873	0.054	0.054	1.598	301	31.0	VEL-2	4.891	0.096	0.072	1.231	310	25.3
VEL-1	3.876	0.038	0.055	0.534	306	31.0	VEL-2	4.922	0.088	0.062	1.218	267	25.0
VEL-1	3.071	0.026	0.044	0.963	312	38.7	VEL-2	4.998	0.112	0.072	1.268	302	24.5
VEL-1	3.338	0.035	0.049	0.898	319	35.4	VEL-2	7.881	0.236	0.113	1.683	292	16.1
VEL-1	2.690	0.035	0.038	0.769	300	43.6	VEL-2	9.638	0.362	0.130	2.987	270	13.5
VEL-1	3.398	0.024	0.047	0.645	305	35.2	VEL-2	6.935	0.332	0.097	3.225	273	17.4
VEL-1	2.474	0.038	0.034	0.860	295	45.9	VEL-3	8.000	0.160	0.113	0.922	296	16.0
VEL-1	2.742	0.041	0.033	0.994	255	43.0	VEL-3	8.034	0.134	0.103	1.159	273	16.1
VEL-1	4.053	0.052	0.051	0.640	269	29.3	VEL-3	6.993	0.151	0.102	1.269	305	18.0
VEL-1	3.459	0.035	0.043	1.024	271	34.7	VEL-3	4.182	0.061	0.056	0.794	286	28.6
VEL-1	4.753	0.042	0.059	0.651	270	25.4	VEL-3	4.655	0.094	0.052	1.604	236	25.3
VEL-1	3.108	0.060	0.045	0.867	307	37.5	VEL-3	3.135	0.043	0.044	0.691	300	37.8
VEL-1	2.412	0.050	0.033	1.315	287	49.2	VEL-3	2.577	0.051	0.038	0.689	307	44.6
VEL-1	6.956	0.018	0.091	1.070	291	19.2	VEL-3	3.365	0.037	0.043	0.617	277	35.1
VEL-1	2.182	0.016	0.034	1.001	341	56.0	VEL-3	4.903	0.170	0.070	1.050	290	22.5
VEL-1	2.556	0.021	0.037	1.035	313	48.2	VEL-3	5.493	0.192	0.079	1.026	289	20.0
VEL-1	6.520	0.029	0.086	1.091	290	20.2	VEL-3	8.423	0.202	0.116	0.731	287	14.1
VEL-1	2.557	0.017	0.038	0.831	324	48.5	VEL-3	10.575	0.244	0.147	0.706	291	11.5
VEL-1	2.568	0.025	0.041	0.881	347	47.2	VEL-3	8.935	0.245	0.126	0.358	290	13.3
VEL-1	3.428	0.027	0.051	0.541	324	36.0	VEL-3	3.617	0.061	0.055	0.647	322	31.7
VEL-2	4.866	0.424	0.075	3.023	270	21.5	VEL-3	2.766	0.033	0.041	0.621	316	41.5
VEL-2	5.846	0.229	0.087	2.665	296	20.6	VEL-3	6.363	0.220	0.090	1.284	284	18.0
VEL-2	5.247	0.239	0.071	3.099	264	22.3	VEL-8	7.970	0.119	0.113	0.437	304	15.6
VEL-2	10.197	0.265	0.122	2.181	248	12.8	VEL-8	7.554	0.116	0.098	0.411	277	16.3
VEL-2	1.680	0.511	0.046	1.819	308	38.1	VEL-8	8.310	0.197	0.125	0.552	312	14.6
VEL-2	2.701	0.055	0.045	0.532	351	39.8	VEL-8	4.943	0.672	0.102	2.452	321	17.8
VEL-2	3.452	0.175	0.050	1.830	279	31.9	VEL-8	7.169	0.554	0.116	1.896	291	14.7

between Velence granite magmatic crystallization and other Western Carpathians A-type occurrences most likely reflects different palaeogeographic position, and therefore different timing of this Permian granite.

The presented xenotime-(Y) in-situ chemical dating reveals post-Variscan age corresponding to the Middle Permian (Guadalupian) stage. However, it is systematically younger (≈ 20 Ma) than magmatic monazite-(Ce) in the host granite. The most plausible interpretations of this age discrepancy are: (1) the xenotime-(Y) age indicates younger, late-magmatic crystallization than the early-magmatic age of monazite-(Ce) precipitation; or (2) post-magmatic (subsolidus) recrystallization of orthomagmatic xenotime-(Y) due to younger event and subsequent overprint of the parental granitic rocks. The age difference between monazite-(Ce) and xenotime-(Y) EPMA chemical ages for the same granite (≈ 20 Ma) is generally too great, thus the second scenario is most likely. Moreover, most xenotime-(Y) crystals show partial alteration and formation of secondary microtexture characterised with occurrence of Th-silicate (thorite?) and/or cheralite inclusions (Fig. 2H, J) and irregular zoning (Fig. 2L). This most likely reflects the dissolution-reprecipitation process (check chapter 5.1.) herein, and connection with rejuvenation. In addition, the 266 ± 5.2 Ma xenotime-(Y) EPMA age is clearly comparable to SHRIMP zircon ages (262 ± 4 Ma – 267 ± 2 Ma) for the Western Carpathian A-type granite occurrences (Turčok, Hrončok and Upohlav; Ondrejka et al., unpubl.). This further suggests that fluid-assisted xenotime-(Y) recrystallization is connected with increased heat transfer during the granites emplacement.

Finally, the rare presence of ca. 670 – 640 Ma old monazite-(Ce) domains indicates admixture of Neoproterozoic material

Table 6: Analytical data and ages of xenotime-(Y) from the investigated samples.

Sample	Th	U	Pb	Y	Age	Age	Sample	Th	U	Pb	Y	Age	Age
	wt.%	wt.%	wt.%	wt.%	(Ma)	2σ		wt.%	wt.%	wt.%	wt.%	(Ma)	2σ
VEL-1	0.617	0.629	0.029	32.881	248	62.2	VEL-2F	0.970	1.093	0.058	31.239	292	38.1
VEL-1	1.275	1.316	0.064	30.444	261	30.4	VEL-2F	1.084	1.376	0.059	31.078	240	31.5
VEL-1	1.258	1.517	0.070	31.263	257	27.3	VEL-2F	0.735	1.577	0.070	31.226	269	29.5
VEL-1	0.693	0.745	0.037	31.632	271	53.5	VEL-2F	1.666	1.758	0.078	30.922	240	23.9
VEL-1	0.728	0.810	0.040	31.856	268	48.7	VEL-2F	1.688	1.749	0.092	31.148	281	24.1
VEL-1	0.601	0.648	0.029	31.479	244	60.6	VEL-8A	0.785	0.850	0.043	41.800	274	46.1
VEL-1	0.618	0.769	0.041	32.300	298	53.3	VEL-8A	1.896	1.353	0.083	41.207	297	26.7
VEL-1	0.556	0.666	0.034	31.067	282	60.6	VEL-8A	1.116	0.876	0.045	41.436	260	41.4
VEL-1	2.097	1.552	0.081	29.645	256	24.1	VEL-8C	0.039	0.575	0.705	41.737	317	56.8
VEL-1	1.577	1.213	0.067	30.553	273	30.8	VEL-8C	0.043	0.678	0.852	45.819	292	47.4
VEL-1	0.438	0.289	0.728	32.484	299	117.2	VEL-8B	0.035	0.654	0.757	43.132	263	52.6
VEL-1	0.724	0.705	0.038	31.621	288	54.2	VEL-8B	0.040	0.741	0.854	42.006	264	46.6
VEL-1	0.980	1.292	0.056	30.635	247	32.3	VEL-8B	0.041	0.529	0.833	41.404	295	50.4
VEL-1	1.644	1.731	0.086	29.615	267	23.4	VEL-8B	0.038	0.520	0.817	41.759	284	51.5
VEL-1	1.146	1.364	0.064	31.581	260	30.0	VEL-8B	0.041	0.258	0.992	45.096	272	47.0
VEL-1	1.155	1.324	0.071	30.240	293	30.8	VEL-8B	0.035	0.500	0.762	42.896	277	54.9
VEL-1	2.491	1.692	0.098	29.272	278	21.3	VEL-8B	0.050	0.459	1.065	45.615	297	41.7
VEL-1	0.768	0.881	0.044	31.938	275	46.3	VEL-8B	0.080	1.079	1.601	44.612	286	26.8
VEL-1	0.485	0.662	0.029	32.034	247	64.5	VEL-8B	0.037	0.865	0.731	43.967	269	50.1
VEL-1	2.246	1.459	0.077	30.045	251	25.2	VEL-8B	0.033	0.820	0.677	43.447	264	54.2
VEL-1	0.617	0.658	0.033	31.360	271	61.0	VEL-8B	0.048	0.960	0.954	43.210	275	40.3
VEL-2F	1.325	1.697	0.080	31.053	264	25.8	VEL-8B	0.047	0.970	0.924	43.004	272	41.2

in the granite protolith. This systematic presence of an older recycled material is also supported by the occurrence of 650 – 630 Ma old inherited zircon cores in the Velence granite dated by SHRIMP method (cf. Uher & Ondrejka, 2009).

Acknowledgments: This work was supported by the Slovak Research and Development Agency under contracts APVV-18-0065, APVV-19-0065 and VEGA Agency Nos. 1/0151/19 and 1/0467/20. We thank V. Kollárová (Bratislava) and S. Kurylo (Banská Bystrica) for providing the EPMA facilities. Finally we thank one anonymous reviewer, Igor Broska (Reviewer), Peter Bačík (Handling Editor) , Rastislav Vojtko (Editorial Board Member) and Martin Bednárik (Executive Editor) for their constructive suggestions.

References

Åmli R., 1975: Mineralogy and rare earth geochemistry of apatite and xenotime from the Gloserheia granite pegmatite, Froland, southern Norway. *American Mineralogist*, 60, 607–620.

Badanina E.V., Trumbull R.B., Dulski P., Wiedenbeck M., Veksler I.V. & Syritso L.F., 2006: The behavior of rare-earth and lithophile trace elements in rare-metal granites: a study of fluorite, melt inclusions and host rocks from the Khangilay complex, Transbaikalia, Russia. *Canadian Mineralogist*, 44, 667–692.

Bagiński B., Jokubauskas P., Domańska-Siuda J., Kartashov P. & MacDonald R., 2016: Hydrothermal metasomatism of a peralkaline granite pegmatite, Khaldzan Buragtag massif, Mongolian Altai; complex evolution of REE-Nb minerals. *Acta Geologica Polonica*, 66, 473–491.

Banfield J.F. & Eggleton R.A., 1989: Apatite replacement and rare earth mobilisation, fractionation, and fixation during weathering. *Clays and Clay Minerals*, 37, 113–127.

Barrat A.J., Zanda B., Moynier F., Bollinger C., Liorzou C. & Bayon G., 2012: Geochemistry of Cl chondrites: major and trace elements and Cu and Zn isotopes. *Geochimica et Cosmochimica Acta*, 83, 79–92.

Bea F., 1996: Resistence of REE, Y, Th and U in granites and crustal protoliths: implications for the chemistry of crustal melts. *Journal of Petrology*, 37, 3, 521–552.

Benkó Zs., Molnár F., Billström K., Pécskay Z. & Lespinasse M., 2010: Genetic and age relationship of base metal mineralization along the Periadriatic-Balaton Lineament system on the basis of radiogenic isotope studies. *Acta Mineralogica Petrographica*, Abstract Series 6, 224.

Benkó Zs., Molnár F., Lespinasse M., Billström K., Pécskay Z. & Németh T., 2014[a]: Triassic fluid mobilization and epigenetic lead-zinc sulphide mineralization in the Transdanubian Shear Zone(Pannonian Basin, Hungary). *Geologica Carpathica*, 65, 177–194.

Benkó Zs., Molnár F., Lespinasse M. & Váczi T., 2014[b]: Evidence for exhumation of granite intrusion in a regional extensional stress regime based on coupled microstructural and fluid inclusion plane studies – An example from the Velence Mts., Hungary. *Journal of Structural Geology*, 65, 44–58.

Bingen B., Demaiffe D. & Hertogen J., 1996: Redistribution of rare earth elements, thorium, and uranium over accessory minerals in the course

of amphibolite to granulite facies metamorphism: the role of apatite and monazite in orthogneisses from southwestern Norway. *Geochimica et Cosmochimica Acta*, 60, 8, 1341–1354.

Braun J.-J., Pagel M., Muller J.-P., Bilong P., Michard A. & Guillet B., 1990: Cerium anomalies in lateritic profiles. *Geochimica et Cosmochimica Acta*, 54, 781–795.

Broska I., 2001: Typomorphic accessory minerals, in Granitic plutonism of the Western Carpathians. *In*: Petrík I., Kohút M. & Broska I. (Eds.): Granitic plutonism of the Western Carpathians–Guide book to Eurogranites 2001, VEDA, Geological Institute, Slovak Academy of Sciences, Bratislava, pp. 36–39.

Broska I. & Kubiš M., 2018: Accessory minerals and evolution of tin-bearing S-type granites in the western segment of the Gemeric Unit (Western Carpathians). *Geologica Carpathica*, 69, 5, 483–497.

Broska I. & Siman P., 1998: The breakdown of monazite in the West-Carpathian Veporic orthogneisses and Tatric granites. *Geologica Carpathica*, 49, 3, 161–167.

Broska I. & Uher P., 1991: Regional typology of zircon and its relationship to allanite/monazite antagonism (on an example of Hercynian granitoids of western Carpathians). *Geologica Carpathica*, 42, 271–277.

Broska I. & Uher P., 2001: Whole-rock chemistry and genetic typology of the West-Carpathian Variscan granites. *Geologica Carpathica*, 52, 2, 79–90.

Broska I., Petrík I. & Uher P., 2012[a]: Accessory minerals of the granitic rocks of the Western Carpathians. Veda Publications, Bratislava, 250 p. [in Slovak with English summary].

Broska I., Petrík I. & Uher P., 2012[b]: Paragenesis of typomorphic accessory minerals vs. typology of granitic rocks: examples from Western Carpathians, Slovakia. *Acta Mineralogica-Petrographica*, Abstract Series, 7, 22 p.

Broska I., Petrík I. & Williams C.T., 2000: Coexisting monazite and allanite in peraluminious granitoids of the Tribeč Mountains, Western Carpathians. *American Mineralogist*, 85, 22–32.

Broska I., Williams C.T. & Hrdlička M., 2006: Behaviour of principal accessory phosphate minerals in the silicic melt of the Western Carpathians. *Mineralogia Polonica*, Special Papers, 28, 30–32.

Broska I., Williams C.T., Janák M. & Nagy G., 2005: Alteration and breakdown of xenotime-(Y) and monazite-(Ce) in granitic rocks of the Western Carpathians, Slovakia. *Lithos*, 82, 71–83.

Buck H.M., Cooper M.A., Černý P., Grice J.D. & Hawthorne F.C., 1999: Xenotime-(Yb), $YbPO_4$, a new mineral species from the Shatford Lake pegmatite group, southeastern Manitoba, Canada. *Canadian Mineralogist*, 37, 1303–1306.

Buda G., 1969: Genesis of granitoid rocks of the Mecsek and Velence Mountains on the basis of the investigation of the feldspars. *Acta Geologica Academiae Scientiarium Hungaricae*, 13, 131–155.

Buda G., 1985: Origin of collision-type Variscan granitoids in Hungary, West Carpathian and Central Bohemian Pluton. Unpublished Ph. D. Thesis, 95 p. [in Hungarian].

Buda G., 1993: Enclaves and fayalite bearing pegmatitic „nests" in the upper part of the granite intrusion of the Velence Mts., Hungary. *Geologica Carpathica,* 44, 3, 143–153.

Buda G. & Nagy G., 1995: Some REE-bearing accessory minerals in two types of Variscan granitoids, Hungary. *Geologica Carpathica*, 46, 2, 67–78.

Budzyń B. & Sláma J., 2019: Partial resetting of U-Pb ages during experimental fluid-induced re-equilibration of xenotime. *Lithos*, 346–347, 105163

Budzyń B., Hetherington C.J., Williams M.L., Jercinovic M.J. & Michalik M., 2010: Fluid mineral interactions and constraints on monazite alteration during metamorphism. *Mineralogical Magazine*, 74, 659–681.

Budzyń B., Harlov D.E., Kozub-Budzyń A.G. & Majka J., 2017: Experimental constraints on relative stabilities of two systems monazite-(Ce) – allanite-(Ce) – fluorapatite and xenotime-(Y) – (Y, HREE)-rich epidote – (Y, HREE)-rich fluorapatite, in high Ca and Na-Ca environments under P-T conditions of 200–1000 MPa and 450–750 °C. *Mineralogy and Petrology*, 111, 183–217.

Budzyń B., Harlov D.E., Williams M.L. & Jercinovic M.J., 2011: Experimental determination of stability relations between monazite, fluorapatite, allanite, and REE-epidote as a function of pressure, temperature, and fluid composition. *American Mineralogist*, 96, 1547–1567.

Budzyń B., Sláma J., Kozub-Budzyń A.G., Konečný P., Holický I., Rzepa G. & Jastrzębski M., 2018: Constraints on the timing of multiple thermal events and re-equilibration recorded by High-U zircon and xenotime: Case study of pegmatite from Piława Górna (Góry Sowie Block, SW Poland). *Lithos,* 310–311, 65–85.

Casillas R., Nagy G., Pantó G., Brandle J. & Fórizs I., 1995: Occurrence of Th, U, Y, Zr and REE-bearing accessory minerals in late-Variscan granitic rocks from the Sierra Guadarrama (Spain). *European Journal of Mineralogy*, 7, 989–1006.

Cherniak D.J., 2006: Pb and rare earth element diffusion in xenotime. *Lithos*, 88, 1–14.

Cherniak D.J., Watson E.B., Grove M. & Harrison T.M., 2004: Pb diffusion in monazite: a combined RBS/SIMS study 1. *Geochimica et Cosmochimica Acta* 68, 829–840.

Cocherie A. & Albarede F., 2001: An improved U-Th-Pb age calculation for electron microprobe dating of monazite. *Geochimica et Cosmochimica Acta*, 65, 24, 4509–4522.

Čopjaková R., Škoda R., Vašinová Galiová M., Novák M. & Cempírek J., 2015: Sc and REE-rich tourmaline replaced by Sc-rich REE-bearing epidote-group mineral from the mixed (NYF plus LCT) Kracovice pegmatite (Moldanubian Zone, Czech Republic). *American Mineralogist*, 100, 1434–1451.

Cuney M. & Friedrich M., 1987: Physicochemical and crystal-chemical controls on accessory mineral paragenesis in granitoids: implications for uranium metallogenesis. *Bulletin de Mineralogie,* 110, 2, 235–247.

Demartin F., Pilati T., Diella V., Donzelli S., Gentile P. & Gramaccioli C.M., 1991[a]: The chemical composition of xenotime from fissures and pegmatites in the Alps. *Canadian Mineralogist*, 29, 69–75.

Demartin F., Pilati T., Diella V., Donzelli S. & Gramaccioli C.M., 1991[b]: Alpine monazite: further data. *Canadian Mineralogist*, 29, 61–67.

Engi M., 2017: Petrochronology based on REE-Minerals: monazite, allanite, xenotime, apatite. *Reviews in Mineralogy and Geochemistry*, 83, 365–418.

Finger F. & Krenn E., 2007: Three metamorphic monazite generations in a high pressure rock from the Bohemian Massif and the potentially important role of apatite in stimulating polyphase monazite growth along a PT loop. *Lithos*, 95, 1–2, 103–115.

Finger F., Broska I., Roberts M.P. & Schermaier A., 1998: Replacement of primary monazite by apatite-allanite-epidote coronas in an amphibolite facies granite gneiss from the eastern Alps. *American Mineralogist*, 83, 3–4, 248–258.

Fisher F.G. & Meyrowitz R., 1962: Brockite, a new calcium thorium phosphate from the Wet Mountains, Colorado. *American Mineralogist*, 47, 1346–1355.

Förster H.J., 1998: The chemical composition of REE-Y-Th-U-rich accessory minerals in peraluminous granites of the Erzgebirge-Fichtelgebirge region, Germany, Part I: the monazite-(Ce)-brabantite solid solution series. *American Mineralogist*, 83, 3–4, 259–272.

Gieré R. & Sorensen S.S., 2004: Allanite and other REE-rich epidote-group minerals. *Reviews in Mineralogy and Geochemistry*, 56, 431–494.

Gramaccioli C.M. & Segalstad T.V., 1978: A uranium- and thorium rich monazite from south-alpine pegmatite at Piona, Italy. *American Mineralogist*, 63, 757–761.

Harlov D.E., 2010: Th and U incorporation into xenotime during partial alteration by alkali-bearing fluids. *Goldschmidt Conference Abstracts*, A382.

Harlov D.E., 2011: Formation of monazite and xenotime inclusions in fluorapatite megacrysts, Gloserheia Granite Pegmatite, Froland, Bamble Sector, southern Norway. *Mineralogy and Petrology*, 102, 77–86.

Harlov D.E., Wirth R. & Förster H.J., 2005: An experimental study of dissolution–reprecipitation in fluorapatite: fluid infiltration and the formation of monazite. *Contributions to Mineralogy and Petrology*, 150, 268–286.

Harlov D.E., Wirth R. & Hetherington C.J, 2007: The relative stability of monazite and huttonite at 300–900 °C and 200–1000 MPa: Metasomatism and the propagation of metastable mineral phases. *American Mineralogist*, 92, 1652–1664.

Hetherington C.J. & Harlov D.E., 2008: Metasomatic thorite and uraninite inclusions in xenotime and monazite from granitic pegmatites, Hidra anorthosite massif, southwestern Norway: mechanics and fluid chemistry. *American Mineralogist*, 93, 806–820.

Hetherington C.J., Jercinovic M.J., Williams M.L. & Mahan K., 2008: Understanding geologic processes with xenotime: Composition, chronology, and a protocol for electron probe microanalysis. *Chemical Geology*, 254, 133–147.

Horváth I., Daridáne Tichy M., Dudko A., Gyalog L. & Ódor L., 2004: Geology of the Velence Hills and the Balatonfő. Geological Institute of Hungary, Budapest, 316 p.

Horváth I., Daridáne Tichy M. & Ódor L., 1983: Magnezittartalmú dolomitos karbonatit (beforszit) telérkőzet a Velencei-hegységből. [Magnesite-bearing dolomite carbonate (beforsite) alluvial rock from the Velence Hills]. *A Magyar* Állami *Földtani Intézet* Évi *Jelentése,* 1981, 369–388 [in Hungarian].

Irber W., 1999: The lanthanide tetrad effect and its correlation with K/hojRb, Eu/Eu*, Sr/Eu, Y/Ho, and Zr/Hf of evolving peraluminous granite suites. *Geochimica et Cosmochimica Acta*, 63, 489–508.

Jantsky B., 1957: Geology of the Velence Mts. *Geologica Hungarica Series Geologica* 10, 166p. [in Hungarian and in French with English summary].

Johan Z. & Johan V., 2005: Accessory minerals of the Cinovec (Zinnwald) granite cupola, Czech Republic: indicators of petrogenetic evolution. *Mineralogy and Petrology*, 83, 1–2, 113–150.

Kelts A.B., Ren M. & Anthony E.Y., 2008: Monazite occurrence, chemistry, and chronology in the granitoid rocks of the Lachlan Fold Belt, Australia: an electron microprobe study. *American Mineralogist*, 93, 373–383.

Konečný P., Kusiak M.A. & Dunkley D.J., 2018: Improving U-Th-Pb electron microprobe dating using monazite age references. *Chemical Geology*, 484, 22–35.

Krenn E. & Finger F., 2007: Formation of monazite and rhabdophane at the expense of allanite during Alpine low temperature retrogression of metapelitic basement rocks from Crete, Greece: microprobe data and geochemical implications. *Lithos*, 95, 1–2, 130–147.

Krenn E., Harlov D.E., Finger F. & Wunder B., 2012: LREE-redistribution among fluorapatite, monazite, and allanite at high pressures and temperatures. *American Mineralogist*, 97, 1881–1890.

Kylander–Clark A.R.C., 2017: Petrochronology by laser–ablation inductively coupled plasma mass spectrometry. *Reviews in Mineralogy and Geochemistry*, 83, 183–198.

Lee D.E. & Bastron H., 1967: Fractionation of rare-earth elements in allanite and monazite as related to geology of the Mt. Wheeler mine area, Nevada. *Geochimica et Cosmichimica Acta*, 31, 339–356.

Lee D.E. & Dodge F.C.W., 1964: Accessory minerals in some granitic rocks in California and Nevada as a function of calcium content. *American Mineralogist*, 49, 1660–1669.

Lee D.E. & Silver L.T., 1964: Accessory minerals in some granitic rocks in California and Nevada as a function of calcium content. *American Mineralogist*, 49, 1660–1670.

Lo Pò D., Braga R., Massonne H.J., Molli G., Montanini A. & Theye T., 2016: Fluid-induced breakdown of monazite in medium-grade metasedimentary rocks of the Pontremoli basement (Northern Apennines, Italy). *Journal of Metamorphic Geology,* 34, 63–84.

MacDonald R., Bagiński B., Kartashov P.M., Zozulya D. & Dzierzanowski P., 2015: Interaction of rare-metal minerals with hydrothermal fluids; evidence from quartz-epidote metasomatites of the Haldzan Buragtag massif, Mongolian Altai. *Canadian Mineralogist*, 53, 1015–1034.

Masau M., Černý P., Cooper M.A., Chapman R. & Grice J.D., 2002: Monazite-(Sm), a new member of the monazite-group from the Annie Claim #3 granitic pegmatite, Southeastern Manitoba. *Canadian Mineralogist*, 40, 1649–1655.

Mayer B.S., Krenn E., & Finger F., 2014: Microcrystals of Th-rich monazite (La) with a negative Ce anomaly in metadiorite and their role for documenting Cretaceous metamorphism in the Slavonian Mountains (Croatia). *Mineralogy and Petrology*, 108, 231–243.

Montel J.M., 1993: A model for monazite/melt equilibrium and application to the generation of granitic magmas. *Chemical Geology*, 110, 127–146.

Montel J.M., Foret S., Vescambre M., Nicollet C. & Provost A., 1996: Electron microprobe dating of monazite. *Chemical Geology*, 131, 37–53.

Nagy G., Draganits E., Demény A., Pantó G. & Árkai P., 2002: Genesis and transformation of monazite, florencite and rhabdophane during medium grade metamorphism: examples from the Sopron Hills, Eastern Alps. *Chemical Geology*, 191, 25–46.

Ni Y., Hughes J.M. & Mariano A.N., 1995: Crystal chemistry of the monazite and xenotime structures. *American Mineralogist*, 80, 21–26.

Ondrejka M., Uher P., Pršek J. & Ozdin D., 2007: Arsenian monazite-(Ce) and xenotime-(Y), REE arsenates and carbonates from the Tisovec- Rejkovo rhyolite, Western Carpathians, Slovakia: composition and substitutions in the $(REE,Y)XO_4$ system (X = P, As, Si, Nb, S). *Lithos*, 95, 116–129.

Ondrejka M., Uher P., Putiš M., Broska I., Bačik P., Konečný P. & Schmiedt I., 2012: Two-stage breakdown of monazite by post-magmatic and metamorphic fluids: an example from the Veporic orthogneiss, Western Carpathians, Slovakia. *Lithos*, 142–143, 245–255.

Ondrejka M., Putiš P., Uher P., Schmiedt I., Pukančík L. & Konečný P., 2016: Fluid-driven destabilization of REE-bearing accessory minerals in the granitic orthogneisses of North Veporic basement (Western Carpathians, Slovakia). *Mineralogy and Petrology*, 110, 561–580.

Ondrejka M., Bačík P., Sobocký T., Uher P., *Škoda* R., Mikuš T., Luptáková J. & Konečný P., 2018: Minerals of the rhabdophane group and the alunite supergroup in microgranite: products of low temperature alteration in a highly acidic enviroment from the Velence Hills, Hungary. *Mineralogical Magazine*, 82, 1277–1300.

Parrish R.R., 1990: U-Pb dating of monazite and its application to geological problems. *Canadian Journal of Earth Sciences*, 27, 1431–1450.

Pérez-Soba C., Vilaseca C., Orejana D. & Jeffries T., 2014: Uranium-rich accessory minerals in the peraluminous and perphosphorous Belvís de Monroy pluton (Iberian Variscan belt). *Contributions to Mineralogy and Petrology*, 167, 1008.

Petrík I. & Konečný P., 2009: Metasomatic replacement of inherited metamorphic monazite in a biotite-garnet granite from the Nízke Tatry Mountains,

Western Carpathians, Slovakia: Chemical dating and evidence for disequilibrium melting. *American Mineralogist*, 94, 957–974.

Plašienka D., Grecula P., Putiš M., Kováč M. & Hovorka D., 1997: Evolution and structure of the Western Carpathians: an overview. *In*: Grecula P., Hovorka D. & Putiš M. (Eds.): Geological evolution of the Western Carpathians. Mineralia Slovaca – Monograph, Bratislava, pp. 1–24.

Putnis A., Hinrichs R., Putnis C.V., Golla-Schindler U. & Collins L.G., 2007: Hematite in porous red-clouded feldspars: evidence of large-scale crustal fluid-rock interaction. *Lithos*, 95, 10–18.

Scherrer N.C., Engi M., Gnos E., Jakob V. & Liechti A., 2000: Monazite analysis; from sample preparation to microprobe age dating and REE quantification. *Schweizeriche Mineralogische und Petrographische Mitteilengen*, 80, 93–105.

Schmitt A.K. & Vazquez J.A., 2017: Secondary ionization mass spectrometry analysis in petrochronology. *Reviews in Mineralogy and Geochemistry*, 83, 199–230.

Snetsinger K.D., 1967: Accessory minerals in some Sierra Nevada granitic rock as a function of calcium content. *American Mineralogist*, 52, 832–842.

Spear F.S. & Pyle J.M., 2002: Apatite, monazite and xenotime in metamorphic rocks. *Reviews in Mineralogy and Geochemistry*, 48, 293–335.

Spear F.S., Pyle J.M. & Cherniak D., 2009: Limitations of chemical dating of monazite. *Chemical Geology*, 266, 218–230.

Spišiak J., Vetráková L., Chew D., Ferenc Š., Mikuš T., Šimonová V. & Bačík P., 2018: Petrology and dating of the Permian lamprophyres from the Malá Fatra Mts. (Western Carpathians, Slovakia). *Geologica Carpathica*, 69, 453–466.

Suzuki K. & Adachi M., 1991: Precambrian provenance and Silurian metamorphism of the Tsubonosawa paragneiss in the South Kitakami terrane, Northeast Japan, revealed by the chemical Th–U–total Pb isochron ages of monazite, zircon and xenotime. *Geochemical Journal*, 25, 357–376.

Suzuki K., Adachi M. & Tanaka T., 1991: Middle Precambrian provenance of Jurassic sandstone in the Mino Terrane, central Japan: Th–U–total Pb evidence from an electron microprobe monazite study. *Sedimentary Geology*, 75, 141–147.

Vozárová A., Larionov A., Šarinová K., Vďačný M., Lepekhina E., Vozár J. & Lvov P., 2018: Detrital zircons from the Hronicum Carboniferous–Permian sandstones (Western Carpathians, Slovakia): depositional age and provenance. *International Journal of Earth Sciences*, 107, 1539–1555.

Uher P. & Broska I., 1995: The Velence Mts. granitic rocks: geochemistry, mineralogy and comparison to Variscan Western Carpathian granitoids. *Acta Geologica Hungarica*, 37, 45–66.

Uher P. & Broska I., 1996: Post-orogenic Permian granitic rocks in the Western Carpathian – Pannonian area: geochemistry, mineralogy and evolution. *Geologica Carpathica*, 47, 311–321.

Uher P. & Ondrejka M., 2009: The Velence granites, Transdanubic Superunit: a product of Permian A-type magmatism and Alpine overprint (results of zircon SHRIMP and monazite EMPA dating). *HunTek 09–7th Meeting of the Central European Tectonic Studies Group (CETeG) & 14th Meeting of the Czech Tectonic Studies Group (ČTS)*, Pécs, Hungary. Hungarian Geological Institute, 57 p.

Uher P., Broska I. & Ondrejka M., 2002: Permian to Triassic granitic and rhyolitic magmatism in the Western Carpathians: composition, evolution and origin. *Geologica Carpathica*, 53 (special issue), 188–189.

Uher P., Ondrejka M. & Konečný P., 2009: Magmatic and post-magmatic Y-REE-Th phosphate, silicate and Nb-Ta-Y-REE oxide minerals in A-type metagranite: an example from Turčok massif, the Western Carpathians, Slovakia. *Mineralogical magazine*, 73, 1009–1025.

Uher P., Kohút M., Ondrejka M., Konečný P. & Siman P., 2014: Monazite-(Ce) in Hercynian granites and pegmatites of the Bratislava Massif, Western Carpathians: compositional variations and Th-U-Pb electron-microprobe dating. *Acta Geologica Slovaca*, 6, 215–231.

Uher P., Ondrejka M., Bačík P., Broska I. & Konečný P., 2015: Britholite, monazite, REE carbonates, and calcite: products of hydrothermal alteration of allanite and apatite in A-type granite from Stupné, Western Carpathians, Slovakia. *Lithos*, 236–237, 212–225.

Upadhyay D. & Pruseth K. L., 2012: Fluid-induced dissolution breakdown of monazite from Tso Morari complex, NW Himalayas: evidence for immobility of trace elements. *Contributions to Mineralogy and Petrology*, 164, 303–316.

Veksler I.V., Dorfman A.M., Kamenetsky M., Dulski P. & Dingwell D.B., 2005: Partitioning of lanthanides and Y between immiscible silicate and fluoride melts, fluorite and cryolite and the origin of the lanthanide tetrad effect in igneous rocks. *Geochimica et Cosmochimica Acta*, 69, 2847–2860.

Whalen J.B., Currie K.L. & Chappell B.W., 1987: A-type granites: geochemical characteristics, discrimination and petrogenesis. *Contribution Mineralogy Petrology*, 95, 407–419.

Whitney D.L. & Evans B.W., 2010: Abbreviations for names of rock-forming minerals. *American Mineralogist*, 95, 185–187.

Williams M.L., Jercinovic M.J., Goncalves P. & Mahan K., 2006: Format and philosophy for collecting, compiling, and reporting microprobe monazite ages. *Chemical Geology*, 225, 15 p.

Zhu X.K. & O`Nions R.K., 1999: Monazite chemical composition: some implications for monazite geochronology. *Contributions to Mineralogy and Petrology*, 137, 351–363.